IL-7-mediated expansion of autologous lymphocytes increases CD8$^+$ T Cell VLA-4 expression and accumulation within glioblastoma

Authors

1. Kirit Singh[1,2]
2. Kelly M. Hotchkiss[1,2]
3. Sarah L. Cook[1,2]
4. Pamy Noldner[3]
5. Ying Zhou[3]
6. Eliese M. Moelker[1,2]
7. Chelsea O. Railton[1,2]
8. Emily E. Blandford[1,2]
9. Bhairavy J. Puviindran[1,2]
10. Shannon E. Wallace[1,2]
11. Pamela K. Norberg[1,2]
12. Gary E. Archer[1,2]
13. Beth Shaz[3]
14. Katayoun Ayasoufi[1,2*]
15. John H. Sampson[1,2**]
16. Mustafa Khasraw[1†, ***]
17. Peter E. Fecci[1,2,4, ***]

[1]The Preston Robert Tisch Brain Tumor Center at Duke University Medical Center, Durham, NC, US.

[2]Department of Neurosurgery, Duke University Medical Center, Durham, NC, US.

[3]The Marcus Center for Cellular Cures, Duke University Medical Center, Durham, NC, US.

[4]Duke Center for Brain and Spine Metastasis.

*Author added to manuscript since initial submission (with consent of all other authors)

**Affiliation now University of Colorado School of Medicine, Anschutz Medical Campus, Aurora, CO.

***These authors contributed equally to the manuscript.

†Co-Corresponding Author: Mustafa Khasraw, M.D.

The Preston Robert Tisch Brain Tumor Center

Duke University | Box 3624, Durham, NC 27710

T +1 919.684.6173 | F +1 919.681.1697

mustafa.khasraw@duke.edu

†Co-Corresponding Author: Peter E. Fecci, M.D., Ph.D.,

The Preston Robert Tisch Brain Tumor Center

Duke University | Box 3050, Durham, NC 27710

T +1 919.681.8977 | F +1 919.684.9045

peter.fecci@duke.edu

Keywords

Immunotherapy; T cells; Cell migration/adhesion

Conflict-of-interest statement

1. KS reports grants paid to his institution and research contracts from Adaptin Bio, which has licensed intellectual property from Duke related to the use of Brain Bi-specific T cell Engagers (BRiTE) and combination autologous lymphocyte therapy.
2. KMH reports no relevant disclosures.
3. SLC reports grants paid to her institution from Immorna Therapeutics, Immvira Therapeutics.
4. PN reports no relevant disclosures.
5. YZ reports no relevant disclosures.

6. EMM reports no relevant disclosures.
7. COR reports no relevant disclosures.
8. EEB reports no relevant disclosures.
9. BP reports no relevant disclosures.
10. SW reports no relevant disclosures.
11. PKN reports no relevant disclosures.
12. GEA reports no relevant disclosures.
13. BS reports no relevant disclosures.
14. KA reports no relevant disclosures.
15. JHS reports an equity interest in Istari Oncology, which has licensed intellectual property from Duke related to the use of poliovirus and D2C7 in the treatment of glioblastoma. JHS is an inventor on patents related to BRiTE, PEP-CMV DC vaccine with tetanus, as well as poliovirus vaccine and D2C7 in the treatment of glioblastoma.
16. MK reports grants paid to his institution, or contracts from BMS, AbbVie, BioNTech, CNS Pharmaceuticals, Daiichi Sankyo Inc., Immorna Therapeutics, Immvira Therapeutics, JAX lab for genomic research, and Personalis Inc. MK also received consulting fees from AnHeart Therapeutics, George Clinical, Manarini Stemline, and Servier and is on a data safety monitoring board for BPG Bio.
17. PEF reports funding from a Cancer Research Institute (CRI) Arash Ferdowsi Lloyd J.Old STAR Award.

83 # Graphical Abstract

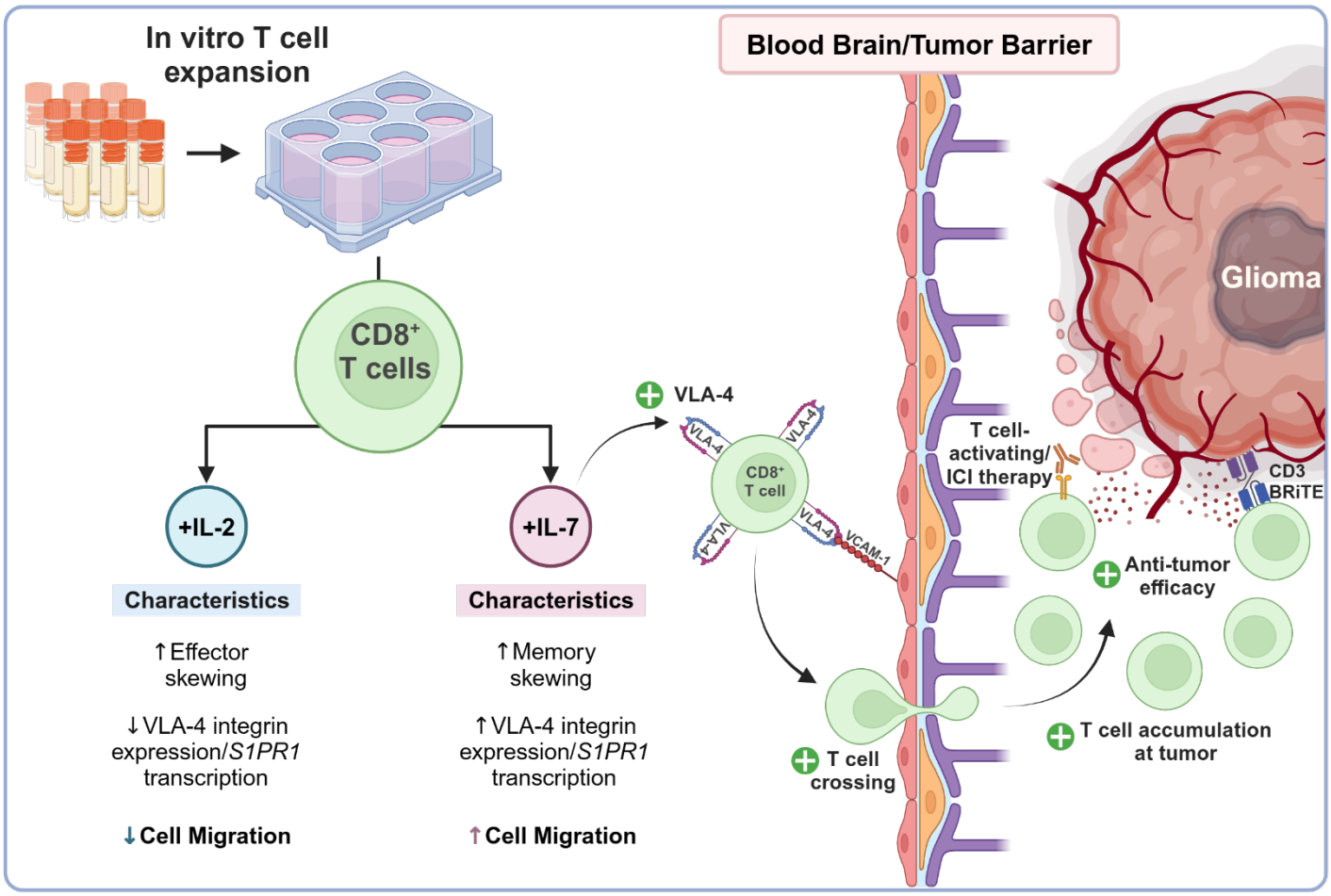

84

85

86

87

88

89

90

91

92

Abstract

The efficacy of T cell-activating therapies against glioma is limited by an immunosuppressive tumor microenvironment and tumor-induced T cell sequestration. We investigated whether peripherally infused non-antigen specific autologous lymphocytes (ALT) could accumulate in intracranial tumors. We observed that non-specific autologous $CD8^+$ ALT cells can indeed accumulate in this context, despite endogenous T cell sequestration in bone marrow. Rates of intratumoral accumulation were significantly increased when expanding lymphocytes with IL-7 compared to IL-2. Pre-treatment with IL-7 ALT also enhanced the efficacy of multiple tumor-specific and non-tumor-specific T cell-dependent immunotherapies against orthotopic murine and human xenograft gliomas. Mechanistically, we detected increased VLA-4 on mouse and human $CD8^+$ T cells following IL-7 expansion, with increased transcription of genes associated with migratory integrin expression (*CD9)*. We also observed that IL-7 increases *S1PR1* transcription in human $CD8^+$ T cells, which we have shown to be protective against tumor-induced T cell sequestration. These observations demonstrate that expansion with IL-7 enhances the capacity of ALT to accumulate within intracranial tumors, and that pre-treatment with IL-7 ALT can boost the efficacy of subsequent T cell-activating therapies against glioma. Our findings will inform the development of future clinical trials where ALT pre-treatment can be combined with T cell-activating therapies.

Brief Summary

T cell immunotherapies are limited by low T cell counts in glioma. Adoptively transferred lymphocytes expanded with IL-7 accumulate in tumors and enhance anti-tumor efficacy.

121 # Introduction

122 T cell-activating immunotherapies, such as immune checkpoint blockade (ICB), require functional T cells at the tumor site
123 to be effective (1-3). Unfortunately, intracranial tumors are harbored within the immunologically distinct central nervous
124 system (CNS) and sit shielded by an immunosuppressive tumor micro-environment (TME) and the blood-brain barrier
125 (BBB) (4). We have shown that CNS tumors, such as glioblastoma, also possess the unique ability to sequester naïve T
126 cells within bone marrow (5), limiting their access to the TME. Likewise, we have more recently described a central role
127 for tumor-associated macrophages (TAM) in driving glioma-infiltrating T cells towards a terminally exhausted state (6),
128 limiting their antitumor capacities (7). Accordingly, high-grade gliomas possess low numbers of tumor infiltrating
129 lymphocytes (TILs (8)) and have proven minimally responsive to ICB in clinical trials (9-11). This paucity of functional TILs
130 will similarly limit the therapeutic efficacy of newer synthetic therapies that rely on endogenous T cells, including brain bi-
131 specific T cell engagers (BRiTEs) (12). Strategies for enhancing functional T cell presence within CNS tumors are needed.
132
133 Currently, strategies to increase T cell numbers in tumor include expanding the T cell pool intratumorally; encouraging T
134 cell trafficking from the periphery; or adding T cells systemically. Each of these face significant challenges. Expansion of
135 local lymphocytes is limited by subsequent severe exhaustion amidst tumor-infiltrating $CD8^+$ T cells, making them less
136 proliferative to stimulation (13). Recruitment of peripheral lymphocytes can be boosted by immunostimulatory cytokines
137 (e.g., IL-7 (14) or IL-12 (15)), but peripheral cytokine administration can induce significant systemic toxicity (16-18). Local
138 administration of cellular therapies or immunostimulatory cytokines is an alternative but requires an invasive procedure,
139 limiting the potential for repeat administrations (19, 20). Ultimately, peripheral infusion of unmodified or CAR-T cells is an
140 established and easily repeatable method of adding lymphocyte populations to tumors within the CNS (21, 22). Modifying
141 this approach, then, we asked whether peripherally infused non-antigen specific autologous lymphocytes would
142 accumulate in established CNS tumors and synergize with T cell-activating/ICB therapies.
143
144 Currently, cellular therapies such as adoptive lymphocyte transfer (ALT) typically use cytokines such as Interleukin-2 (IL-
145 2) or IL-7 to support *ex vivo* T cell expansion (23). IL-2 skews lymphocytes towards a terminally differentiated T effector
146 (T_{EFF}) phenotype. While T_{EFF} cells do express migratory integrins, they often have a short half-life once removed from
147 culture (24, 25). IL-7, in turn, promotes homeostatic T cell expansion and expands the central memory T cell (T_{CM}) pool,
148 leading to greater T cell persistence in vivo (26, 27). Peripheral administration of long-acting IL-7 has been shown to
149 enhance T cell accumulation in murine glioma and boosts the efficacy of T cell engagers against solid tumors (14, 28). We

therefore sought to evaluate which growth factor might produce a cellular product with favorable BBB-penetrance and enhanced anti-tumor efficacy in models of established intracranial glioma.

Herein, we report that peripherally administered T cells (ALT) lacking antigen specificity accumulate in established murine intracranial tumors, despite tumor-imposed T cell sequestration in bone marrow. Rates of intratumoral accumulation are significantly increased when T cells are expanded with IL-7 (IL-7-ALT), which also increases the efficacy of accompanying immunotherapeutic platforms. We find that IL-7 increases expression of the migratory integrin Very Late Antigen-4 (VLA-4) on both mouse and human $CD8^+$ T cells, while VLA-4 blockade abrogates the enhanced accumulation of IL-7-ALT in tumors. Transcriptional analysis of hPBMCs expanded with IL-7 reveals upregulation of genes involved in integrin expression and tumor infiltration (*CD9, VLA-6, EPHA4).* Also upregulated is *S1PR1* (sphingosine-1-phosphate receptor 1, also described as S1P1), increased levels of which are known to avert T cell sequestration and license immunotherapeutic responses to glioma (5). These results provide a route to optimizing ALT expansion, as well as to using ALT as an immunotherapeutic adjunct.

176 # Results

177 ## IL-7-expanded CD8$^+$ T cells demonstrate increased accumulation within orthotopic glioblastoma
178 models despite endogenous T cell sequestration in bone marrow

179

180 Though peripherally administered, activated autologous T cells have been shown to cross the BBB under physiologic
181 conditions (29), their ability to enter the CNS in the setting of tumor-directed T cell sequestration was unclear. Previous
182 work by our group established that sequestration predominantly impacts naïve T cells (endogenous or ALT), while memory
183 T cells are largely unperturbed (5). We therefore began by examining the rate of CNS tumor accumulation for *ex vivo*-
184 expanded non-specific autologous T cells.

185

186 First, we developed T cell expansion processes that skewed phenotypes towards effector (T_{EFF}, CD44^{high}CD62L^{low}) or
187 central memory (T_{CM}, CD44^{high}CD62L^{high}) subsets. Expansion of T cells with either 100IU/mL IL-2 or 20ng/mL IL-7 was
188 chosen to enrich for CD8$^+$ T_{EFF} or CD8$^+$ T_{CM} phenotypes, respectively, based on prior experience and published protocols
189 (23, 30, 31). Following expansion, flow cytometry was performed to assess the makeup of the ALT product pre-
190 administration (gating and expansion strategy in Figure S1, A and B). *Ex vivo* expansions with both IL-2 and IL-7 yielded
191 a cellular product of >95% CD3$^+$ cells (Figure S1C) which predominantly consisted of CD8$^+$ T cells (~80%, Figure S1D).
192 The IL-2-ALT product was preferentially skewed towards T_{EFF} (Figure S1E) while the IL-7-ALT product skewed towards
193 T_{CM} (Figure S1F). Few naïve CD8$^+$ T cells (T_N, CD44^{low}CD62L^{high}) were present at the end of expansion with either cytokine
194 (Figure S1G).

195

196 To establish the trafficking capabilities of non-specific CD45.1$^+$ T cells in the setting of tumor, we intracranially implanted
197 CT2A stably transfected with the glioma-specific neoantigen Epidermal Growth Factor Receptor variant III (EGFRvIII) into
198 congenic CD45.2$^+$ C57/BL6 mice. CT2A is syngeneic on the C57 background and exhibits high heterogeneity, stemness,
199 and resistance to therapy (32). We have also previously described tumor-induced T cell sequestration in bone marrow
200 using this model (5).

201

202 After tumors were well-established at 13 days, mice were given a single ALT of either IL-2 or IL-7-expanded CD45.1$^+$ T
203 cells (Figure 1A). Following ALT, tumor and bone marrow were collected daily from separate mice over 4 days. Flow
204 cytometry was used to measure changes to the viable exogenous (CD45.1$^+$) and endogenous (CD45.2$^+$) CD3$^+$ T cell

205 compartment (flow gating in Figure S2A). By 48-hours post administration, we detected an increased proportion of the IL-
206 7-ALT dose within tumor compared to IL-2-ALT. (Figure 1B, IL-7-ALT vs IL-2-ALT in tumor, $p<0.05$*). No significant
207 difference between dose proportions in bone marrow was seen at the same timepoint (Figure 1B, $p=0.8172$). Examination
208 of intratumoral T cells over time found that accumulation rates for IL-7-ALT $CD8^+$ but not $CD4^+$ lymphocytes were
209 significantly greater than for IL-2-ALT. In both groups, endogenous $CD8^+$ T cell populations in tumor declined (time course
210 shown for $CD4^+$ T cells in Figure 1C, $CD8^+$ T cells in Figure 1D. 48-hour IL-7-ALT $CD8^+$ T cells 31.24x vs IL-2-ALT 4.14x
211 $p<0.01$**, 72-hour IL-7-ALT $CD8^+$ T cells 42.2x vs IL-2-ALT 5.88x, $p<0.01$**). Counts of IL-7-ALT $CD8^+$ T cells in tumor
212 were also increased compared to IL-2-ALT throughout, though differences were non-significant (Figure S2B).
213
214 Simultaneously, increases in endogenous $CD4^+$ and $CD8^+$ T cell populations in bone marrow were seen across groups
215 over time ($CD4^+$ T cells in Figure 1E, $CD8^+$ T cells in Figure 1F). Greater fold-change increases in endogenous $CD4^+$ T
216 cell accumulation in bone marrow were observed compared to $CD8^+$ T cells, in keeping with previous descriptions of
217 tumor-induced $CD4^+$ T cell sequestration (endogenous $CD4^+$ fold-change of 2.69x vs $CD8^+$ T cells fold change of 1.76x at
218 72-hr observation point (5, 33, 34)). ALT entry into bone marrow was also observed, although this was restricted to the
219 $CD8^+$ population. Rates of ALT accumulation in bone marrow did not differ between expansion conditions (Figure 1F, non-
220 adjusted IL-7-ALT $CD8^+$ T cell counts in Fig. S2C). Increases in spleen weights were also seen following ALT, before a
221 subsequent precipitous decline below baseline (time course in Figure 1G). We concluded then that non-antigen specific,
222 exogenously administered $CD8^+$ T cells can indeed accumulate within glioma despite tumor-imposed T cell sequestration,
223 with IL-7-ALT accumulating intratumorally at a greater rate than IL-2-ALT.
224

225 IL-7-ALT synergizes with T cell-centric immunotherapies in orthotopic glioma models

226
227 We next examined whether IL-2 or IL-7 ALT would each enhance survival when combined with T cell-activating
228 immunotherapies. In a first set of experiments, we combined each ALT with EGFRvIII-BRiTE in a U87 xenograft model
229 stably transfected with EGFRvIII (U87vIII). EGFRvIII-BRiTE is a bi-specific T cell engager possessing specificity for both
230 the CD3 receptor and the glioma-specific antigen EGFRvIII (35). As EGFRvIII-BRiTE is fully humanized, we evaluated
231 efficacy in a NOD scid gamma (NSG) mouse model reconstituted with either IL-7- or IL-2-expanded human (h)PBMCs.
232 We observed that IL-7 ALT yielded a significant but modest survival benefit when combined with BRiTE, compared to the
233 IL-2-ALT-BRITE combination (Figure 2A, $p<0.05$*). Interestingly, no differences between the two modalities were observed
234 in vitro (Figure 2B).

235

236 Having observed a survival benefit with the combination of IL-7-ALT + BRITE, we looked to see how successfully IL-7-
237 ALT might also combine with various checkpoint or T cell activity modifying therapies that typically have limited or no
238 success in CT2A models (outline in Figure 2C). After CT2AvIII tumors established for 10 days, animals were treated with
239 IL-7 ALT alone, or in combination with αCTLA-4 (antagonist), αPD-1 (antagonist) or α4-1BB (agonist) monoclonal
240 antibodies. We observed a small trend toward prolonged survival when combining IL-7 ALT with αPD-1 therapy (2/6 mice
241 surviving > 30 days, 0/6 with long term overall survival), but a significant increase in survival when combining IL-7-ALT +
242 α4-1BB compared to IL-7-ALT only (Figure 2D, $p<0.05$*). We therefore selected the IL-7-ALT + α4-1BB combination
243 approach for further experiments in this model and performed controlled survival studies using the same timing schematic
244 as above (Figure 2E). We again found that IL-7-ALT + α4-1BB therapy yielded a significant survival benefit, this time
245 compared to combination IL-2-ALT and α4-1BB ($p<0.05$*); α4-1BB alone ($p<0.05$*); either IL-2 or IL-7-ALT only (both
246 $p<0.01$**); or to untreated controls ($p<0.01$**). Interestingly, while combination IL-7 ALT + αPD-1 therapy exhibited a limited
247 survival benefit in the CT2AvIII glioma model (Figure 2D), greater efficacy was observed in mice bearing more
248 immunogenic GL261 gliomas (36) (Figure 2F).

249

250 We likewise evaluated whether adding IL-7 ALT to clinically relevant checkpoint blockade therapy would result in toxicity.
251 Body weights during and for two weeks following treatment were recorded in the GL261-bearing mice whose survival is
252 depicted in Figure 2F. No differences between groups were seen (Figure 2G). To evaluate toxicity in greater detail, we
253 performed acute toxicity studies in healthy mice receiving IL-7 + αPD-1 therapy, comparing against sham controls (outline
254 shown in Figure S3A). Body weights again remained stable throughout (Figure S3B). Five days after treatment-end, blood,
255 liver tissue, spinal cord and brain were taken to assess for liver function, changes in cellular architecture and potential
256 demyelination. No significant difference in serum chemistry was seen between groups (Figure S3C). Review of brain and
257 spinal cord by a board-certified veterinary pathologist also found no differences in terms of histological features, cellular
258 architecture, or demyelination (representative photomicrographs in Figure S3, D and E). Regarding liver, no
259 histopathologic abnormalities related to lymphocytic infiltration were noted in the sham group, though presumed peri-
260 mortem acute hepatocellular apoptosis/necrosis without associated inflammation was seen in 2 of 5 animals. In the
261 combination group, pathologist review identified small numbers of randomly distributed foci (1 to 4 per animal) of acute to
262 subacute hepatocellular apoptosis/necrosis associated with a mixed lymphocytic infiltrate (representative
263 photomicrographs in Figure S3F). While these findings were considered to be treatment-related effects, they were
264 considered unlikely to indicate systemic toxicity given the unchanged liver function tests.

265 ## IL-7-expanded CD8$^+$ T cells accumulating in tumor exhibit both central and effector memory
266 phenotypes

267

268 Frequent antigenic stimulation upregulates trafficking molecules on T_{CM} cells (37, 38), while T_{EFF} cells also upregulate
269 migratory ligands such as LFA-1 and VLA-4, enhancing endothelial binding following activation (24, 25). We therefore
270 evaluated the phenotypic makeup of exogenous T cells that entered the brain following ALT, as well as their expression of
271 migratory integrins.

272

273 To begin, we intravenously administered CD45.1$^+$ IL-2-ALT or IL-7-ALT to CD45.2$^+$ mice with established (15-day) CT2AvIII
274 tumors. Tumors were collected 3- and 48-hours post ALT (outline in Figure 3A). Again, we observed significantly enhanced
275 accumulation of IL-7-ALT CD8$^+$ T cells compared to IL-2-ALT (Figure 3B, 3-hrs $p<0.01$**, 48-hrs $p<0.001$***). Similar to
276 previous findings, ALT in tumor primarily consisted of CD8$^+$ T cells (Figure 3C, CD8$^+$ vs CD4$^+$ T cells, $p<0.0001$****). By
277 the 48-hour timepoint, IL-7-ALT T cells made up approximately ~20% of all T cells in tumor, (Figure 3D, mean 18.8%, SD
278 ±4.3%, n=5), while the fraction of T cells that consisted of IL-2-ALT in tumor was ~1% (mean 1.7%, SD ±1.5%, n=4).

279

280 Evaluating the phenotypic composition of the CD8$^+$ T cells infiltrating tumor, we observed that at 48-hours post ALT
281 administration, the endogenous CD8$^+$ T cell phenotypes in tumor were similar, regardless of whether ALT was expanded
282 with IL-2 or IL-7. Phenotypes consisted mainly of effector (T_{EFF}) cells (Figure 3E). Regarding administered (exogenous)
283 ALT CD8$^+$ T cells, IL-2-ALT in tumor also pre-dominantly consisted of T_{EFF} cells, while IL-7-ALT consisted of a mixed
284 central/effector (T_{CM}/T_{EFF}) population (Figure 3F). Naïve populations were negligible and did not vary between groups.
285 Given this, we considered that enhanced entry or retention might be more characteristic of the T_{CM} population. However,
286 we noted that the make-up of ALT in tumor was similar to the phenotypic make-up of the IL-2 and IL-7 ALT cell product
287 pre-administration (IL-2-ALT in vitro (pre-administration) vs. in vivo (post-administration) in Figure 3G; IL-7-ALT in Figure
288 3H). This led us to consider instead whether the increased fraction of CD8$^+$ T_{CM} in tumor for the IL-7-ALT group simply
289 reflected the composition of the pre-administration product.

290

291 To clarify, we compared accumulation of the CD8$^+$ T_{CM} and T_{EFF} subsets between both ALT groups. Both the IL-7-ALT
292 CD8$^+$ T_{EFF} and T_{CM} subsets were present in tumor in significantly greater numbers than their IL-2-ALT counterparts
293 (individual subsets for each ALT condition in Figures 3I and 3J, comparison between ALT conditions in Figure 3K, IL-7-

294 ALT vs IL-2-ALT T_{CM} and T_{EFF} p<0.0001****). We concluded that enhanced accumulation of IL-7-ALT CD8$^+$ T cells in tumor
295 was more a feature of IL-7 expansion, and not reflective of T_{CM} phenotype.
296

297 Expansion with IL-7 upregulates expression of the pro-migratory integrin VLA-4 on murine CD8$^+$ T 298 cells, which is required for enhanced intratumoral accumulation

299

300 To better understand the impact of IL-7 on T cell accumulation in tumor, we analyzed the expression of migratory integrins
301 common to all lymphocytes (VLA-4, LFA-1) on exogenous T cells that entered the CNS using flow cytometry (gating
302 strategy in Figure 4A). We observed that both the expression of the migratory integrin VLA-4 and the fraction of VLA-4^{Hi}
303 cells was significantly increased amidst IL-7-ALT CD8$^+$ T cells arriving early in tumor compared to IL-2-ALT, though this
304 difference subsided by the 48-hour sampling point (gMFI in Figure 4B, 3-hrs & 48-hrs p<0.01**, CD8$^+$ T cell VLA-4^{Hi} % in
305 Figure 4C). Conversely, we saw increased LFA-1 expression on IL-2-ALT CD8$^+$ T cells compared to IL-7-ALT at the first
306 sampling timepoint (Figure 4D, p<0.01** LFA-1 gating in Figure S4A). The percentage of CD8$^+$ LFA-1^{Hi} T cells was similarly
307 high throughout for both conditions (Figure 4E). The pre-administration fraction of CD8$^+$ VLA-4^{Hi} T cells was also higher
308 amidst the IL-7-ALT, while the fraction of pre-administration CD8$^+$ LFA-1^{Hi} T cells was similar between groups (CD8$^+$ VLA-
309 4^{Hi} T cells in Figure 4F, CD8$^+$ LFA-1^{Hi} T cells in Figure 4G, technical repeats for each ALT condition shown).
310

311 To evaluate the impact of VLA-4 levels on T cell trafficking to tumor, we again used IL-7 to generate an ALT consisting of
312 CD4$^+$ and CD8$^+$ T cells that had increased VLA-4 expression compared to baseline levels seen when expanding with IL-
313 2 (VLA-4^{Hi} or VLA-4^{Lo} ALT, pooled ALT expression shown in Figure S4B). VLA-4^{Hi} or VLA-4^{Lo} ALT were then separately
314 administered to animals with 15-day established CT2AvIII tumors, either alone or alongside a VLA-4 blocking antibody
315 (BioXCell, 200μg intraperitoneally (IP)). VLA-4^{Hi} ALT CD8$^+$ T cells demonstrated significantly enhanced accumulation
316 within tumor compared to VLA-4^{Lo} ALT, accumulation that was abrogated by co-administration of αVLA-4 (VLA-4^{Hi} vs VLA-
317 4^{Lo}, p<0.05*; VLA-4^{Hi} vs αVLA-4 & VLA-4^{Hi}, p<0.05*, 3 pooled experiments shown, Figure 4H). Administration of αVLA-4
318 was also found to reduce the therapeutic efficacy of combination IL-7-ALT + α4-1BB seen in the CT2AvIII model. Here,
319 we observed that IP αVLA-4 reduced survival in the combination therapy group from 54 to 30 days, similar to monotherapy
320 groups, though these curves were not significantly different (IP α4-1BB only: 37 days, 3 pooled experiments shown, Figure
321 4I). Based on these findings, we concluded that: (1) IL-7 exposure increases the expression of VLA-4 on CD8$^+$ T cells and
322 (2) VLA-4 expression and signaling are necessary for the enhanced accumulation of IL-7 ALT CD8$^+$ T cells in glioma.

323 ## Intratumoral lymphocytic VLA-4 and endothelial/pericytic VCAM-1 expression increase over time in
324 glioma

325

326 While evaluating ALT VLA-4 expression, we noted that VLA-4 levels were consistently elevated over time on endogenous
327 $CD8^+$ T cells in tumor (Figure 5A). Noting the role of VLA-4 in guiding T cells towards inflamed tissue (39), we first examined
328 whether VLA-4^{Hi} T cells were unique to the tumor environment. We performed flow cytometry on various tissues (brain,
329 spleen, bone marrow, lungs, and blood) in mice with established CT-2AvIII tumors or sham-injected controls (experimental
330 outline in Figure 5B, gating strategy in Figure S5A). Animals did not receive ALT, allowing for evaluation of endogenous T
331 cell VLA-4 expression without external influence. We again observed a significant increase to the VLA-4^{Hi} fraction amidst
332 $CD8^+$ T cells, as well as to weight-adjusted VLA-4^{Hi} $CD8^+$ T cell counts in brain tumor tissue compared to all other
333 compartments, as well as to brain from sham controls (fractions in Figure 5C, comparisons in Figure 5D, $p<0.0001$****,
334 weight adjusted counts vs sham controls in Figure S5B, $p<0.01$**). VLA-4^{Hi} $CD8^+$ T cells in tumor were overwhelmingly
335 T_{EFF} cells (Figure S5C). Outside of the tumor, VLA-4^{Hi} $CD8^+$ T cells were most commonly found in the bone marrow (Figure
336 5, C and D).

337

338 As glioblastoma is characterized by high levels of microvascular proliferation (40), we next evaluated if endothelial/pericytic
339 VCAM-1 (VLA-4's ligand (41)) was also increased in tumor. Recent studies of T cell recruitment in other intracranial tumor
340 models (i.e., melanoma) found negligible VCAM-1^+ endothelial or pericyte populations (42). To determine if VCAM-1^+ cells
341 were present in the context of glioma, we collected brain tissue from mice with established intracranial CT2AvIII glioma or
342 sham-controls. Both endothelial cell ($CD31^+CD13^-$) and pericyte ($CD31^-CD13^+$) populations were analyzed via flow
343 cytometry (outline in Figure 5E, gating in Figure S5D). Here, we observed a similar frequency of expression of VCAM-1
344 on endothelial cells and pericytes on Day 12 of tumor growth (~45%$^+$), with similar levels also seen across tumor and
345 sham (Figure 5F). However, as tumors progressed further, increasing proportions and counts of VCAM-1^+ endothelial cells
346 and pericytes were observed in tumor compared to sham (Figure 5G, pericytes $p<0.05$*, endothelial cells $p<0.01$**, D17
347 weight adjusted counts in Figure 5, H and I respectively).

348

349 Given this, we questioned whether intratumoral T cell accumulation might be enhanced by blocking the VLA-4-VCAM-1
350 axis, and whether results would differ if blockade was administered systemically vs. intracranially. To evaluate, we
351 implanted mice with CT2AvIII gliomas, and 13 days later administered αVLA-4 either intraperitoneally or intracranially. As
352 free αVLA-4 antibody levels are 100-fold reduced in cerebro-spinal fluid (CSF) compared to serum following systemic

353 infusion (43), we selected dose levels of 200 µg αVLA-4 intraperitoneally and 2 µg intracranially to achieve approximately
354 equivalent exposure (experiment outline in Figure 5J). First, we evaluated the impact of both intraperitoneal and
355 intracranial αVLA-4 on intratumoral $CD8^+$ T cell VLA-4 expression and found that both suppressed VLA-4 levels on T cells,
356 though this was only sustained when administering intraperitoneally (Figure S5E). Next, we evaluated intracranial counts
357 of endogenous $CD4^+$ and $CD8^+$ T cell populations 24- and 72-hrs post αVLA-4 administration. Across treatment groups,
358 no differences were seen at the 24-hour measurement point (Figure S5F). By 72-hours, however, intraperitoneal αVLA-4
359 had elicited reduced counts of both $CD4^+$ and $CD8^+$ T cells in tumors, even compared to non-tumor-bearing controls (24-
360 hr intratumoral counts in Figure S5F, 72-hr counts in Figure 5K, intraperitoneal αVLA-4 vs sham, $CD4^+$ and $CD8^+$ T cells,
361 $p<0.05$*). Conversely, intracranial αVLA-4 produced increases in accumulation of both populations within tumors by 72-
362 hrs post administration, though this was only significant for $CD4^+$ T cells compared to sham controls (Figure 5K, intracranial
363 αVLA-4 vs sham, $CD4^+$ T cells $p<0.05$*, $CD8^+$ T cells $p=0.068$).
364
365 We therefore further investigated the therapeutic potential for intracranial VLA-4 blockade. While increasing intratumoral
366 T cell counts remains a central goal, VLA-4 is involved in immune synapse formation and T cell activation (44), making
367 the net impact of its blockade unclear. To evaluate the effects of VLA-4 blockade on T cell activity, we performed in vitro
368 co-culture cytotoxicity assays with CT2AvIII, T cells, and EGFRvIII-BRiTE. αVLA-4 antibody was added at escalating
369 amounts to BRiTE at its EC_{50} dose (0.01µg/mL, dose-finding data in Figure S5G). The addition of αVLA-4 indeed inhibited
370 the T cell anti-tumor cytotoxicity otherwise mediated by BRiTE (Figure 5L). Thus, while intracranial αVLA-4 may enhance
371 intratumoral T cell accumulation, there appears to be a negative impact on anti-tumor cytotoxicity.
372

373 IL-7 expansion of hPBMCs from both healthy volunteers and patients with glioblastoma upregulates 374 lymphocyte VLA-4 expression

375
376 We therefore returned to further investigate our initial IL-7-ALT method for enhancing T cell numbers in tumor. To determine
377 the clinical translatability of our approach, we sought to determine whether a) leukapheresis products from patients with
378 glioblastoma would respond / expand to the same extent as those from healthy controls, and b) similar changes to VLA-4
379 expression and T cell migratory potential would occur when expanding human T cells in the presence of IL-7.
380
381 To permit relevant comparisons, we obtained leukapheresis products from healthy volunteers and patients with
382 glioblastoma who had given written consent to provide PBMCs for the purposes of T cell expansion. An overview of donor

383 demographics and pathology is shown in Table 1. Median ages across groups were similar (controls 54.3 yrs (range 43.3–
384 55.4) vs glioblastoma 58.7 yrs (range 37.4–63.3)) with a 2:1 M:F ratio in both groups. Of the glioblastoma samples, 5 of 6
385 were collected from patients who had previously received dexamethasone.
386
387 Samples from control and glioblastoma groups were thawed and activated via αCD3/αCD8 stimulation. Cultures were
388 maintained for 14 days in media supplemented with 300 IU/mL IL-2 (based on prior protocols (45)) or 20 ng/mL IL-7. After
389 expansion, cell counts, phenotypes, activation levels and VLA-4 expression were evaluated (flow gating and schematic in
390 Figure S6, A and B). While both IL-7 and IL-2 were capable of independently supporting T cell proliferation (Figure 6A),
391 IL-2 produced greater T cell yields for both control and GBM leukapheresis samples (Figure S6C). Perhaps surprisingly,
392 no significant difference between control and glioblastoma T cell expansion rates were observed. The final expanded
393 product consisted of ~95% $CD3^+$ T cells across all groups (Figure S6D). IL-7 expansion skewed significantly more towards
394 $CD4^+$ T cells (~60:40 ratio of $CD4^+$:$CD8^+$ T cells), whereas IL-2 skewed more towards $CD8^+$ T cells ($CD4^+$:$CD8^+$ T cells ~
395 33:66, Figure 6, B-D). On more specific phenotyping of memory and effector subsets, we observed that T_{EFF} ($CD45RO^-$
396 $CD45RA^+CD95^+CCR7^-$) and T Effector Memory ($T_{EM,}$ $CD45RO^+CD45RA^-CD62L^-CCR7^-$) fractions were similar across the
397 IL-2 and IL-7 expansion groups (T_{EFF} in Figure S6E, T_{EM} in Figure S6F, all subsets in Figure 6E). IL-7 did trend toward
398 increasing the stem cell memory fraction ($T_{SCM,}$ $CD45RO^-CD45RA^+CD95^+CCR7^+$) compared to IL-2, though changes were
399 non-significant (Figure 6F).
400
401 We next evaluated whether IL-7 increased VLA-4 expression on human T cells, as we had seen in our mouse models.
402 We observed a biphasic distribution in VLA-4^+ cells and classed lymphocytes as VLA-4^{Neg}, VLA-4^{Lo} or VLA-4^{Hi} (gating in
403 Figure 6G). For both control and glioblastoma samples, IL-7 significantly increased the VLA-4^{Hi} fraction over that seen with
404 IL-2 (Figure 6H, $p<0.001$***, $CD4^+$ and $CD8^+$ T cell gMFI shown in Figure S6, G & H). Significant upregulation of VLA-4
405 expression was observed on $CD8^+$ T_{EFF} and $CD8^+$ T_{SCM} subsets from both groups (Figure 6, I and J, $p<0.01$** for healthy
406 controls and $p<0.001$*** for glioblastoma patients). Changes to $CD8^+$ T_{EM} VLA-4 expression were non-significant (Figure
407 S6I).
408
409 Finally, we performed in vitro functional assays. These included cytotoxicity assays using our end-expansion product,
410 cultured alongside BRiTE and $EGFRvIII^+$ positive tumor (U87vIII), as described above. Similar dose-dependent tumor
411 killing was observed across all conditions above BRiTE concentrations of 10^3 pg/mL (Figure 6K). We then undertook in
412 vitro stimulation assays of sorted $CD8^+$ T cells (cytokine gating strategy in Figure S7A, sort gating in Figure S7B). Sorted

413 CD8$^+$ T cells were expanded with IL-2 or IL-7 and co-cultured with tumor only (U87vIII); tumor + BRiTE; or phorbol
414 myristate acetate (PMA)/ionomycin. T cells not exposed to tumor, BRiTE or PMA were also analyzed to assess background
415 activity. We observed similar results for IL-2- and IL-7-expanded glioblastoma patient CD8$^+$ T cells in terms of CD107a^{Hi}
416 degranulation, interferon-gamma (IFN-γ), and tumor-necrosis factor-alpha (TNF-α) production (Figure 6, L-N). While we
417 did observe increased frequencies of Granzyme B$^+$ (GzmB$^+$) T cells in the IL-2-expanded group compared to those
418 expanded with IL-7, we also noted an increased baseline frequency of GzmB$^+$ T cells in the unstimulated / IL-2-expanded
419 and tumor only control groups (Figure 6O). Ultimately, then, IL-7 expansion enhanced CD8$^+$ T cell VLA-4 expression
420 amongst hPBMC samples in a manner similar to that seen with murine T cells, while having a similar impact on T cell
421 function to IL-2 exposure.
422

423 IL-7 increases transcription of genes in T cells associated with enhanced migratory function (*CD9*)
424 and protection against sequestration (*S1PR1)*

425

426 To evaluate IL-7's effect on migratory integrin expression, we performed bulk RNA sequencing using the same
427 glioblastoma hPBMC samples. CD8$^+$ T cells were sorted from naïve (pre-expansion), IL-2-expanded, or IL-7-expanded
428 products. Principal component analysis revealed that expansion with IL-7 vs. IL-2 resulted in distinct CD8$^+$ T cell
429 transcriptional fates (Figure 7, A-C). Deeper interrogation of these fates via analysis of differential gene expression
430 revealed that IL-7 significantly increases the transcription of genes involved in T cell migration and trafficking compared to
431 IL-2 (*EPHA4* (adjusted p (p_{adj})= 9.39E-27(46)), *ITGA4* (VLA-4, p_{adj}=0.043) and *ITGA6* (VLA-6, p_{adj}=9.64E-08 (47))). Genes
432 involved in stem-like/memory T cell development were also significantly increased by IL-7 exposure (*TCF7* which encodes
433 for TCF1, p_{adj}=1.60E-06 (48), *FOXO1,* p_{adj}=7.52E-11 and *LEF1*, p_{adj}=2.41E-10). IL-2-expanded CD8$^+$ T cells demonstrated
434 increased transcription of T cell markers associated with effector activity (*CD69,* p_{adj}=2.48E-34, *GZMB,* p_{adj}=2.16E-18) and
435 exhaustion (*CTLA-4,* p_{adj}=1.55E-33, *TOX* p_{adj}=0.00068, *HAVCR2* (TIM-3) p_{adj}=0.00018). Volcano plots for all three
436 comparisons are shown in Figure S8, A and B (naïve vs IL-2 or IL-7, respectively), and Figure 7D (IL-2- vs IL-7-expanded).
437 Analysis of raw transcripts per million (TPM) also found that IL-7 yielded the highest TPM for *ITGA4* (VLA-4), but this was
438 not significantly increased compared to the IL-2 cohort (Figure S8C).
439

440 Differential expression analysis also revealed a highly significant outlier when expanding with IL-2 vs IL-7. Transcription
441 of Dual-Specificity Phosphatase 6 (*DUSP6*) was increased 6.8x when expanding with IL-2 vs IL-7 (Figure 7D, p= 7.85E-
442 258). DUSP6 has been shown to negatively regulate the extracellular signal-regulated kinase (ERK1/2) pathway (49-51),

443 which is activated by IL-2 (52). Curious as to the impact of DUSP6, we performed a repeat 2-week expansion where
444 hPBMCs were expanded with IL-2 alone, or alongside BCI, a small molecule inhibitor of DUSP6 (53). We found that while
445 BCI did not increase $CD8^+$ T cell VLA-4 expression, it did increase the fraction of $CD8^+$ T_{SCM} cells ($CD8^+$ T cell VLA-4 gMFI
446 in Figure S8D, $CD8^+$ T_{SCM} fraction in Figure S8E, technical repeats). We surmised that DUSP6 may affect $CD8^+$ T cell
447 differentiation, but not VLA-4 expression.
448
449 Noting that transcription of another migratory integrin (VLA-6) was enhanced with IL-7, we considered whether broader
450 changes in integrin expression might be occurring. We performed hierarchical cluster heatmapping of genes that were
451 differentially expressed across the naïve, IL-2 and IL-7 groups. This identified seven clusters (I-VII, Figure 7E). Clusters I
452 and VI were specifically upregulated in the IL-2-expanded samples, while cluster V was upregulated for both. Cluster IV
453 was the only gene set specifically upregulated within IL-7-expanded samples. To interrogate the biological processes that
454 these clusters represented, we performed Gene Ontology (GO) analysis using the NIH DAVID database (54). For clusters
455 I and VI (upregulated in IL-2), we identified biological processes associated with an inflammatory adaptive immune
456 response and positive regulation of T cell activation (Figure S8, F and G). These included genes related to cytotoxic T cell
457 activity (*GZMA, GZMB, IFNγ, FASLG, CD69*) as well as markers of T cell exhaustion (*CTLA-4, TOX*). For cluster V
458 (upregulated in both), increased transcription of genes associated with cell division were observed (e.g., *MKI67 (55),*
459 Figure S8H).
460
461 GO analysis of cluster IV (upregulated in IL-7) identified biological processes associated with positive regulation of cell
462 migration (Figure 7F). These included genes encoding for *ITGA6* (VLA-6, TPM comparisons across groups shown in
463 Figure 7G) as well as *CD9*, a protein that has been associated with increased expression of multiple migratory integrins,
464 including VLA-6 and VLA-4 (56, 57). Within our data, *CD9* TPM was significantly and specifically increased within IL-7
465 expanded hPBMCs compared to naïve or IL-2 expanded cohorts ($p<0.01$**, Figure 7H). Interestingly, we also identified
466 *S1PR1* (encoding the S1P1 receptor) within cluster IV. Our group has previously reported that loss of S1P1 mediates
467 tumor-induced T cell sequestration in bone marrow (5) and that stabilization of S1P1 on the surface of T cells makes them
468 resistant to sequestration (5). Here, we find that IL-2 significantly reduced *S1PR1* TPM compared to naïve controls
469 ($p<0.05$*), while IL-7 significantly increased *S1PR1* TPM ($p<0.001$***, Figure 7I). We concluded that IL-7 upregulates
470 genes associated with migratory integrin expression, while also increasing *S1PR1* transcription.
471
472

473 # Discussion

474 For T cell-activating therapies to be effective against tumors of the CNS, they must be able to encounter functional immune
475 cells within the intracranial compartment. Although immune cells can cross the BBB (29), primary CNS malignancies are
476 capable of "driving" T cells away by inducing loss of lymphocytic S1P1, resulting in T cell sequestration within bone marrow
477 (5, 58).
478
479 Our results demonstrate that non-specific $CD8^+$ T cells expanded with IL-7 can accumulate in tumor tissue, despite tumor-
480 induced T cell sequestration. Further, we demonstrate that administration of IL-7-ALT can synergize with multiple T cell-
481 activating therapies against established intracranial glioma. Campian et al. reported a related phenomenon, whereby
482 peripheral administration of long-acting recombinant IL-7 enhanced cytotoxic $CD8^+$ T cell numbers systemically and in
483 tumor for similar animal glioma models (14). Another recent study by Lee et al. reports synergism between recombinant
484 IL-7 administration and bi-specific T cell engager therapy in solid tumor models (28). Interestingly, they report that IL-7
485 encourages recruitment of non-exhausted polyclonal bystander $CD8^+$ TILs to tumors. Though these bystander TILs do not
486 have direct anti-tumor activity themselves, they can be redirected by T cell engagers to become tumoricidal. Our study
487 adds to this body of literature, finding that IL-7 enhances expression of migratory integrins like VLA-4, and increases
488 transcription of genes involved in resistance to sequestration (*S1PR1*).
489
490 IL-7's effect on upregulating VLA-4 has been previously reported in vitro (59), and peripheral administration of recombinant
491 human IL-7 (rhIL-7) has been observed to increase VLA-4 and T cell trafficking in murine models of sepsis (60). In our
492 study, RNA sequencing of IL-7-expanded PBMCs from glioblastoma patients revealed increased transcription of genes
493 *(CD9)* associated with enhanced expression of multiple migratory integrins, including VLA-4 and VLA-6 (56, 57). We also
494 have previously identified that S1P1 loss mediates T cell sequestration (5). Accordingly, mice with genetically stabilized
495 S1P1 expression in T cells prove sequestration-resistant and experience prolonged survival to immunotherapy in the face
496 of glioma (5). Our findings align with this prior work. Notably, we also identify that IL-2 exposure significantly decreases
497 the transcription of *S1PR1*. This in turn may underlie some of the failure of IL-2-expanded cellular products to accumulate
498 in intracranial tumors, though further confirmatory work is required.
499
500 We also report here increasing lymphocyte VLA-4 expression and increasing numbers of $VCAM\text{-}1^+$ endothelial
501 cells/pericytes in the context of glioma over the course of tumor progression. Given that recent studies have reported low

502 fractions of VCAM-1^{+} cells in other intracranial malignancies (melanoma (42)), this finding suggests that T cell recruitment
503 and BBB trafficking dynamics may vary between cancer types. To identify disease-specific approaches for enhancing T
504 cell accumulation in tumors of the CNS, further evaluation of VCAM-1^{+} expression across multiple tumor types is
505 warranted. Nevertheless, our findings suggest that for intracranial glioma, VLA-4^{Hi} lymphocytes may be able to encounter
506 VCAM-1 and accumulate in tumor.
507
508 To better reflect the capacity for clinical translation, we confirmed that IL-7 exposure upregulated VLA-4 expression on
509 hPBMCs from both healthy donors and patients with glioblastoma. While we observed reduced yields and less CD8^{+} T
510 cell skewing when expanding hPBMCs with IL-7, we did find that IL-7-cultured hCD8^{+} T cells exhibited similar in vitro
511 functionality to those being IL-2-cultured. Further optimization could include sorting infiltrative (VLA-4^{Hi}) CD8^{+} T cells pre-
512 administration. This might also permit administering a reduced dose to patients, or one with more efficient tumor uptake.
513 In our study, the percentage of the administered ALT dose which entered the brain was small, in keeping with other studies
514 evaluating IV CAR-T therapy against murine CNS malignancy models (<1%, lymphoma (61)). While our approach did not
515 induce significant toxicity/demyelination in brain or spinal cord when combining IL-7-ALT with αPD-1, we did observe a
516 few scattered foci of hepatic cellular apoptosis/necrosis associated with lymphocytic infiltrate. An optimized VLA-4^{Hi}
517 population could reduce the ALT dose required for efficacy, and limit non-CNS organ infiltration.
518
519 A key limitation of our study is that we only evaluated the cytokines IL-2 and IL-7, as we have previously established that
520 they can independently support T cell expansion (23). Similarly, we used doses of IL-2 and IL-7 that known to expand T
521 cells from both mice and humans. However, cytokines such as IL-15, IL-18, IL-21 and others have been used in varying
522 doses to supplement lymphocyte expansion (62). We also note that the IL-7 receptor is downregulated after sustained
523 exposure, and intermittent cycling with IL-7 may enhance the cytokine's effects (63). Our study is confined to evaluating
524 these two cytokines at the specified concentrations and exposure schedules. However, given the vast number of possible
525 permutations, determining the optimal combination, concentration, and timing for cytokine supplementation is beyond the
526 scope of this manuscript and may require a continuous process-development effort.
527
528 In conclusion, we find that expansion of autologous T lymphocytes with IL-7 enhances the ability of CD8^{+} T cells to
529 accumulate within intracranial glioma, even in the setting of tumor-imposed T cell sequestration. Combination IL-7-ALT
530 and T cell-centric immunotherapies increase survival in multiple models of glioma. Analysis of migratory integrins on
531 lymphocytes finds that IL-7 increases CD8^{+} T cell expression of VLA-4. RNAseq analysis finds that IL-7 increases

532 transcription of genes associated with increased migratory integrin expression *(CD9)* as well as *S1PR1*, a G protein-
533 coupled receptor whose stable expression on lymphocytes protects against their sequestration. These findings will be
534 used to inform future clinical trials, where ALT pre-treatment will be combined with T cell-activating therapies targeting
535 glioblastoma (e.g., BRiTE, NCT04903795).
536
537
538
539
540
541
542
543
544
545
546
547
548
549
550
551
552
553
554
555
556
557
558
559
560
561

562 # Materials and Methods

563 ## Sex as a biological variable

564 For pre-clinical in vivo studies, we exclusively used females as CT-2A was established in female mice (64) and superior
565 engraftment of human hematopoietic stem cells has been observed in female NOD-*scid* gamma (NSG) mice (65).
566 Evaluation of clinical samples from volunteers and glioblastoma patients used hPBMCs from males and females (**Table**
567 **1**). Further demographic information in terms of reporting race and ethnicity were based on classifications within the
568 electronic medical records system where available and categorized according to NIH policy (notice number: NOT-OD-15-
569 089).
570

571 ## Mice

572 All mouse strains used, and housing conditions are described within the Supplemental Methods.
573

574 ## Cell lines

575 The origin and validation of CT2A, U87MG, GL261 and transfected sublines are described within the Supplemental
576 Methods.
577

578 ## Murine lymphocyte culturing

579 Expansion processes for murine $CD3^+$ cells are described within the Supplemental Methods.
580

581 ## Leukapheresis and human PBMC culturing

582 Human PBMC collection, processing and expansion are described within the Supplemental Methods.
583

584 ## Tumor inoculation

585 All tumor studies in this report placed tumors intracranially in mice and followed protocols described previously (66), which
586 are described within the Supplemental Methods.
587

588 ## In vivo adoptive lymphocyte transfer and antibody administration

589 For adoptive lymphocyte transfer in this study, cells that had been expanded as described in the murine lymphocyte
590 culturing section were administered as described within the Supplemental Methods.
591

592 ## Tissue processing and flow cytometry

593 Procedures for tissue processing and flow cytometry are based on our previously published protocols (4) and are
594 described within the Supplemental Methods.
595

596 ## Cytotoxicity

597 Tumor cells were labelled with a viability dye before co-culture. The process is described within the Supplemental Methods.
598

599 ## Immune functional assays

600 Immune functional assays were performed with flow-sorted human $CD8^+$ T cells and is described within the Supplemental
601 Methods.
602

603 ## Immunohistochemistry & toxicity

604 Toxicity studies were conducted in C57/Bl6 mice. Processing procedures are described within the Supplemental Methods.
605

606 ## RNA sequencing assays and analysis

607 Flow-sorted $CD8^+$ T cells were snap frozen in cell pellets and analyzed via bulkRNA sequencing at Azenta life sciences.
608 Analysis is described within the Supplemental Methods. PCA analysis was generated using BioJupies (67). Hierarchical
609 cluster heatmaps were generated via the same method and using clustergrammer (Maayan lab, (68)). Gene Ontology
610 (GO) biological processes analysis was performed using the NIH database for annotation, visualization and integrated
611 discovery dashboard (DAVID (54)). Volcano plots were generated based on tests for differential expression (Wald test
612 used to generate p-values and log2 fold changes) created with DESeq2 (69) and visualized using VolcaNoseR (70).
613

614 ## Statistics and reproducibility

615 Experimental results are presented as mean ± SEM unless otherwise stated. Statistical tests for all studies were completed
616 using GraphPad v.10.3.1 (Prism). For comparisons in a single graph, 2-tailed Student's t test or nonparametric Mann-
617 Whitney U test was used, and for multiple comparisons, ANOVA (one-way or two-way) with Holm–Šidák correction for
618 multiple comparisons. Asterisks represent the significance level of any difference (*p<0.05, **p≤0.01, ***p<0.001,
619 ****p<0.0001, p>0.05 not significant). Sample sizes were selected due to practical considerations, with no formal power
620 calculations performed. Efficacy studies following animals for survival were assessed for significance using a log-rank
621 (Mantel-Cox) test. Independent study results were pooled if the effect of replication did not cause significant variation as
622 assessed by two-way ANOVA. All animals were randomized within genotype prior to treatment following tumor
623 implantation. Survival was monitored with the assistance of technicians from the Duke Division of Laboratory Animal
624 Resources (DLAR) who were blinded to study groups and followed animals to endpoint.
625

626 ## Study approval

627 All animal experiments were performed under Duke University IACUC experimental protocol (ID: A163-21-08). Stored
628 anonymized human samples used were collected from glioblastoma patients or volunteers who provided written consent
629 to undergo leukapheresis for T cell expansion for research (glioblastoma donors: Duke IRB #Pro00069444; Duke IRB
630 #Pro00083828; healthy donors: Duke IRB #Pro00009403; approval for secondary analysis: Duke IRB #Pro00117663).
631

632 ## Graphical illustrations

633 The graphical abstract and experimental outlines in Figs. 1, 2, 3, 5, 6, S1, S3 and S7 were created with BioRender.com
634 and exported under a paid license.
635

636 ## Data Availability

637 Values for underlying data for all figures are available in the supporting data values file. RNAseq data (raw counts and
638 processed TPM) has been deposited on the NCBI Gene Expression Omnibus (GEO) repository pending review.
639

640 ## Author Contributions

641 Design, acquisition, analysis of data, and writing of manuscript: KS with assistance from KMH, SLC, PN, YZ,
642 EM, COR, EEB, BJP, SEW, PKN, GEA, BS, JHS, MK and PEF. Overall supervision throughout by JHS, MK
643 and PEF.

644

645 ## Acknowledgements

646 The authors have been supported by the following grants to Duke University: P50-CA190991 (SPORE) (JHS, MK), P01-
647 CA225622 (JHS, MK), U01-NS090284 (JHS), R01-NS099463 (JHS), R01-CA175517 (JHS), and R01-CA235612 (JHS,
648 MK) as well as a Structured Research Agreement with Adaptin Bio (KS, MK). The authors also wish to express their
649 gratitude to Dr. Rebecca Bacon and Dr. Ivan Spasojevic at Duke University Medical Center for their assistance with toxicity
650 studies.

651
652
653
654
655
656
657
658
659
660
661
662
663
664
665
666
667
668

669 # References

670 1. Belmontes B, Sawant DV, Zhong W, Tan H, Kaul A, Aeffner F, et al. Immunotherapy combinations overcome
671 resistance to bispecific T cell engager treatment in T cell-cold solid tumors. *Science Translational Medicine.*
672 2021;13(608):eabd1524.
673 2. Woroniecka KI, Rhodin KE, Dechant C, Cui X, Chongsathidkiet P, Wilkinson D, et al. 4-1BB Agonism Averts TIL
674 Exhaustion and Licenses PD-1 Blockade in Glioblastoma and Other Intracranial Cancers. *Clinical cancer*
675 *research : an official journal of the American Association for Cancer Research.* 2020;26(6):1349-58.
676 3. Baeuerle PA, and Wesche H. T-cell-engaging antibodies for the treatment of solid tumors: challenges and
677 opportunities. *Curr Opin Oncol.* 2022;34(5):552-8.
678 4. Tomaszewski WH, Waibl-Polania J, Miggelbrink AM, Chakraborty MA, Fecci PE, Sampson JH, et al. Broad
679 immunophenotyping of the murine brain tumor microenvironment. *Journal of Immunological Methods.*
680 2021;499:113158.
681 5. Chongsathidkiet P, Jackson C, Koyama S, Loebel F, Cui X, Farber SH, et al. Sequestration of T cells in bone
682 marrow in the setting of glioblastoma and other intracranial tumors. *Nat Med.* 2018;24(9):1459-68.
683 6. Waibl Polania J, Hoyt-Miggelbrink A, Tomaszewski WH, Wachsmuth LP, Lorrey SJ, Wilkinson DS, et al. Antigen
684 presentation by tumor-associated macrophages drives T cells from a progenitor exhaustion state to terminal
685 exhaustion. *Immunity.* 2024.
686 7. Woroniecka K, Chongsathidkiet P, Rhodin K, Kemeny H, Dechant C, Farber SH, et al. T-Cell Exhaustion
687 Signatures Vary with Tumor Type and Are Severe in Glioblastoma. *Clinical cancer research : an official journal of*
688 *the American Association for Cancer Research.* 2018;24(17):4175-86.
689 8. Maddison K, Graves MC, Bowden NA, Fay M, Vilain RE, Faulkner S, et al. Low tumour-infiltrating lymphocyte
690 density in primary and recurrent glioblastoma. *Oncotarget.* 2021;12(21):2177-87.
691 9. Reardon DA, Brandes AA, Omuro A, Mulholland P, Lim M, Wick A, et al. Effect of Nivolumab vs Bevacizumab in
692 Patients With Recurrent Glioblastoma: The CheckMate 143 Phase 3 Randomized Clinical Trial. *JAMA Oncology.*
693 2020;6(7):1003-10.
694 10. Omuro A, Brandes AA, Carpentier AF, Idbaih A, Reardon DA, Cloughesy T, et al. Radiotherapy combined with
695 nivolumab or temozolomide for newly diagnosed glioblastoma with unmethylated MGMT promoter: An
696 international randomized phase III trial. *Neuro-oncology.* 2023;25(1):123-34.

697 11. Lim M, Weller M, Idbaih A, Steinbach J, Finocchiaro G, Raval RR, et al. Phase III trial of chemoradiotherapy with
698 temozolomide plus nivolumab or placebo for newly diagnosed glioblastoma with methylated MGMT promoter.
699 *Neuro-oncology.* 2022;24(11):1935-49.
700 12. Gedeon PC, Schaller TH, Chitneni SK, Choi BD, Kuan CT, Suryadevara CM, et al. A Rationally Designed Fully
701 Human EGFRvIII:CD3-Targeted Bispecific Antibody Redirects Human T Cells to Treat Patient-derived
702 Intracerebral Malignant Glioma. *Clinical cancer research : an official journal of the American Association for*
703 *Cancer Research.* 2018;24(15):3611-31.
704 13. Woroniecka K, Chongsathidkiet P, Rhodin K, Kemeny H, Dechant C, Farber SH, et al. T-Cell Exhaustion
705 Signatures Vary with Tumor Type and Are Severe in Glioblastoma. *Clinical cancer research : an official journal of*
706 *the American Association for Cancer Research.* 2018;24(17):4175-86.
707 14. Campian JL, Ghosh S, Kapoor V, Yan R, Thotala S, Jash A, et al. Long-Acting Recombinant Human Interleukin-
708 7, NT-I7, Increases Cytotoxic CD8 T Cells and Enhances Survival in Mouse Glioma Models. *Clinical Cancer*
709 *Research.* 2022;28(6):1229-39.
710 15. Agliardi G, Liuzzi AR, Hotblack A, De Feo D, Núñez N, Stowe CL, et al. Intratumoral IL-12 delivery empowers
711 CAR-T cell immunotherapy in a pre-clinical model of glioblastoma. *Nature Communications.* 2021;12(1):444.
712 16. Leonard JP, Sherman ML, Fisher GL, Buchanan LJ, Larsen G, Atkins MB, et al. Effects of single-dose
713 interleukin-12 exposure on interleukin-12-associated toxicity and interferon-gamma production. *Blood.*
714 1997;90(7):2541-8.
715 17. Zhang L, Morgan RA, Beane JD, Zheng Z, Dudley ME, Kassim SH, et al. Tumor-infiltrating lymphocytes
716 genetically engineered with an inducible gene encoding interleukin-12 for the immunotherapy of metastatic
717 melanoma. *Clinical cancer research : an official journal of the American Association for Cancer Research.*
718 2015;21(10):2278-88.
719 18. Taylor CA, Watson RA, Tong O, Ye W, Nassiri I, Gilchrist JJ, et al. IL7 genetic variation and toxicity to immune
720 checkpoint blockade in patients with melanoma. *Nature Medicine.* 2022;28(12):2592-600.
721 19. Bagley SJ, Logun M, Fraietta JA, Wang X, Desai AS, Bagley LJ, et al. Intrathecal bivalent CAR T cells targeting
722 EGFR and IL13Rα2 in recurrent glioblastoma: phase 1 trial interim results. *Nature Medicine.* 2024.
723 20. Choi BD, Gerstner ER, Frigault MJ, Leick MB, Mount CW, Balaj L, et al. Intraventricular CARv3-TEAM-E T Cells
724 in Recurrent Glioblastoma. *New England Journal of Medicine.* 2024.

725 21. Bagley SJ, Binder ZA, Lamrani L, Marinari E, Desai AS, Nasrallah MP, et al. Repeated peripheral infusions of
726 anti-EGFRvIII CAR T cells in combination with pembrolizumab show no efficacy in glioblastoma: a phase 1 trial.
727 *Nature Cancer.* 2024.
728 22. O'Rourke DM, Nasrallah MP, Desai A, Melenhorst JJ, Mansfield K, Morrissette JJD, et al. A single dose of
729 peripherally infused EGFRvIII-directed CAR T cells mediates antigen loss and induces adaptive resistance in
730 patients with recurrent glioblastoma. *Sci Transl Med.* 2017;9(399).
731 23. Yang S, Archer GE, Flores CE, Mitchell DA, and Sampson JH. A cytokine cocktail directly modulates the
732 phenotype of DC-enriched anti-tumor T cells to convey potent anti-tumor activities in a murine model. *Cancer*
733 *immunology, immunotherapy : CII.* 2013;62(11):1649-62.
734 24. Ley K, and Kansas GS. Selectins in T-cell recruitment to non-lymphoid tissues and sites of inflammation. *Nat*
735 *Rev Immunol.* 2004;4(5):325-35.
736 25. Nolz JC, Starbeck-Miller GR, and Harty JT. Naive, effector and memory CD8 T-cell trafficking: parallels and
737 distinctions. *Immunotherapy.* 2011;3(10):1223-33.
738 26. Chen D, Tang TX, Deng H, Yang XP, and Tang ZH. Interleukin-7 Biology and Its Effects on Immune Cells:
739 Mediator of Generation, Differentiation, Survival, and Homeostasis. *Front Immunol.* 2021;12:747324.
740 27. Capitini CM, Chisti AA, and Mackall CL. Modulating T-cell homeostasis with IL-7: preclinical and clinical studies.
741 *J Intern Med.* 2009;266(2):141-53.
742 28. Lee K-J, Choi D, Tae N, Song HW, Kang Y-W, Lee M, et al. IL-7-primed bystander CD8 tumor-infiltrating
743 lymphocytes optimize the antitumor efficacy of T cell engager immunotherapy. *Cell Reports Medicine.*
744 2024;5(5).
745 29. Hickey WF, Hsu BL, and Kimura H. T-lymphocyte entry into the central nervous system. *Journal of Neuroscience*
746 *Research.* 1991;28(2):254-60.
747 30. Hinrichs CS, Spolski R, Paulos CM, Gattinoni L, Kerstann KW, Palmer DC, et al. IL-2 and IL-21 confer opposing
748 differentiation programs to CD8+ T cells for adoptive immunotherapy. *Blood.* 2008;111(11):5326-33.
749 31. Markley JC, and Sadelain M. IL-7 and IL-21 are superior to IL-2 and IL-15 in promoting human T cell–mediated
750 rejection of systemic lymphoma in immunodeficient mice. *Blood.* 2010;115(17):3508-19.
751 32. Oh T, Fakurnejad S, Sayegh ET, Clark AJ, Ivan ME, Sun MZ, et al. Immunocompetent murine models for the
752 study of glioblastoma immunotherapy. *J Transl Med.* 2014;12:107.

753 33. Tritz ZP, Ayasoufi K, Malo C, Himes B, Khadka R, Yokanovich L, et al. Combination immunotherapy of αPD-1
754 and extended half-life IL-2 clears established GL261 gliomas in an MHC class I independent fashion. *The*
755 *Journal of Immunology.* 2020;204(1 Supplement):169.15-.15.
756 34. Ayasoufi K, Pfaller CK, Evgin L, Khadka RH, Tritz ZP, Goddery EN, et al. Brain cancer induces systemic
757 immunosuppression through release of non-steroid soluble mediators. *Brain.* 2020;143(12):3629-52.
758 35. Choi BD, Kuan C-T, Cai M, Archer GE, Mitchell DA, Gedeon PC, et al. Systemic administration of a bispecific
759 antibody targeting EGFRvIII successfully treats intracerebral glioma. *Proceedings of the National Academy of*
760 *Sciences.* 2013;110(1):270-5.
761 36. Noffsinger B, Witter A, Sheybani N, Xiao A, Manigat L, Zhong Q, et al. Technical choices significantly alter the
762 adaptive immune response against immunocompetent murine gliomas in a model-dependent manner. *J*
763 *Neurooncol.* 2021;154(2):145-57.
764 37. Kohlmeier JE, Miller SC, Smith J, Lu B, Gerard C, Cookenham T, et al. The chemokine receptor CCR5 plays a
765 key role in the early memory CD8+ T cell response to respiratory virus infections. *Immunity.* 2008;29(1):101-13.
766 38. Ray SJ, Franki SN, Pierce RH, Dimitrova S, Koteliansky V, Sprague AG, et al. The collagen binding alpha1beta1
767 integrin VLA-1 regulates CD8 T cell-mediated immune protection against heterologous influenza infection.
768 *Immunity.* 2004;20(2):167-79.
769 39. Savino W, Chaves B, Bonomo AC, and Cotta-de-Almeida V. Integrin-directed antibody-based immunotherapy:
770 focus on VLA-4. *Immunotherapy Advances.* 2021;1(1).
771 40. Das S, and Marsden PA. Angiogenesis in glioblastoma. *The New England journal of medicine.*
772 2013;369(16):1561-3.
773 41. Singh K, Hotchkiss KM, Patel KK, Wilkinson DS, Mohan AA, Cook SL, et al. Enhancing T Cell Chemotaxis and
774 Infiltration in Glioblastoma. *Cancers (Basel).* 2021;13(21).
775 42. Messmer JM, Thommek C, Piechutta M, Venkataramani V, Wehner R, Westphal D, et al. T lymphocyte
776 recruitment to melanoma brain tumors depends on distinct venous vessels. *Immunity.* 2024;57(11):2688-
777 703.e11.
778 43. Sehr T, Proschmann U, Thomas K, Marggraf M, Straube E, Reichmann H, et al. New insights into the
779 pharmacokinetics and pharmacodynamics of natalizumab treatment for patients with multiple sclerosis, obtained
780 from clinical and in vitro studies. *Journal of Neuroinflammation.* 2016;13(1):164.

781 44. Mittelbrunn M, Molina A, Escribese MM, Yáñez-Mó M, Escudero E, Ursa Á, et al. VLA-4 integrin concentrates at
782 the peripheral supramolecular activation complex of the immune synapse and drives T helper 1 responses.
783 *Proceedings of the National Academy of Sciences.* 2004;101(30):11058-63.
784 45. Miao H, Choi BD, Suryadevara CM, Sanchez-Perez L, Yang S, De Leon G, et al. EGFRvIII-specific chimeric
785 antigen receptor T cells migrate to and kill tumor deposits infiltrating the brain parenchyma in an invasive
786 xenograft model of glioblastoma. *PLoS One.* 2014;9(4):e94281.
787 46. Holen HL, Nustad K, and Aasheim HC. Activation of EphA receptors on CD4+CD45RO+ memory cells
788 stimulates migration. *J Leukoc Biol.* 2010;87(6):1059-68.
789 47. Kitayama J, Ikeda S, Kumagai K, Saito H, and Nagawa H. α6β1 Integrin (VLA-6) Mediates Leukocyte Tether and
790 Arrest on Laminin under Physiological Shear Flow. *Cellular Immunology.* 2000;199(2):97-103.
791 48. Escobar G, Mangani D, and Anderson AC. T cell factor 1: A master regulator of the T cell response in disease.
792 *Sci Immunol.* 2020;5(53).
793 49. Johnson GL, and Lapadat R. Mitogen-activated protein kinase pathways mediated by ERK, JNK, and p38
794 protein kinases. *Science.* 2002;298(5600):1911-2.
795 50. Yoo DH, Im YS, Oh JY, Gil D, and Kim Y-O. DUSP6 is a memory retention feedback regulator of ERK signaling
796 for cellular resilience of human pluripotent stem cells in response to dissociation. *Scientific Reports.*
797 2023;13(1):5683.
798 51. Caunt CJ, and Keyse SM. Dual-specificity MAP kinase phosphatases (MKPs). *The FEBS Journal.*
799 2013;280(2):489-504.
800 52. Yu T-K, Caudell EG, Smid C, and Grimm EA. IL-2 Activation of NK Cells: Involvement of MKK1/2/ERK But Not
801 p38 Kinase Pathway1. *The Journal of Immunology.* 2000;164(12):6244-51.
802 53. Kong T, Laranjeira ABA, Yang K, Fisher DAC, Yu L, Poittevin De La Frégonnière L, et al. DUSP6 mediates
803 resistance to JAK2 inhibition and drives leukemic progression. *Nature Cancer.* 2023;4(1):108-27.
804 54. Sherman BT, Hao M, Qiu J, Jiao X, Baseler MW, Lane HC, et al. DAVID: a web server for functional enrichment
805 analysis and functional annotation of gene lists (2021 update). *Nucleic Acids Res.* 2022;50(W1):W216-w21.
806 55. Uxa S, Castillo-Binder P, Kohler R, Stangner K, Müller GA, and Engeland K. Ki-67 gene expression. *Cell Death*
807 *& Differentiation.* 2021;28(12):3357-70.
808 56. Scherberich A, Moog S, Haan-Archipoff G, Azorsa DO, Lanza F, and Beretz A. Tetraspanin CD9 Is Associated
809 With Very Late–Acting Integrins in Human Vascular Smooth Muscle Cells and Modulates Collagen Matrix
810 Reorganization. *Arteriosclerosis, Thrombosis, and Vascular Biology.* 1998;18(11):1691-7.

811 57. Rubinstein E, le Naour F, Billard M, Prenant M, and Boucheix C. CD9 antigen is an accessory subunit of the
812 VLA integrin complexes. *European Journal of Immunology.* 1994;24(12):3005-13.
813 58. Mrdjen D, Pavlovic A, Hartmann FJ, Schreiner B, Utz SG, Leung BP, et al. High-Dimensional Single-Cell
814 Mapping of Central Nervous System Immune Cells Reveals Distinct Myeloid Subsets in Health, Aging, and
815 Disease. *Immunity.* 2018;48(2):380-95.e6.
816 59. Kitazawa H, Muegge K, Badolato R, Wang JM, Fogler WE, Ferris DK, et al. IL-7 activates alpha4beta1 integrin
817 in murine thymocytes. *The Journal of Immunology.* 1997;159(5):2259-64.
818 60. Unsinger J, McGlynn M, Kasten KR, Hoekzema AS, Watanabe E, Muenzer JT, et al. IL-7 Promotes T Cell
819 Viability, Trafficking, and Functionality and Improves Survival in Sepsis. *The Journal of Immunology.*
820 2010;184(7):3768-79.
821 61. Mulazzani M, Fräßle SP, von Mücke-Heim I, Langer S, Zhou X, Ishikawa-Ankerhold H, et al. Long-term in vivo
822 microscopy of CAR T cell dynamics during eradication of CNS lymphoma in mice. *Proceedings of the National*
823 *Academy of Sciences.* 2019;116(48):24275-84.
824 62. Xu XJ, Song DG, Poussin M, Ye Q, Sharma P, Rodríguez-García A, et al. Multiparameter comparative analysis
825 reveals differential impacts of various cytokines on CART cell phenotype and function ex vivo and in vivo.
826 *Oncotarget.* 2016;7(50):82354-68.
827 63. Vranjkovic A, Crawley AM, Gee K, Kumar A, and Angel JB. IL-7 decreases IL-7 receptor alpha (CD127)
828 expression and induces the shedding of CD127 by human CD8+ T cells. *Int Immunol.* 2007;19(12):1329-39.
829 64. Martínez-Murillo R, and Martínez A. Standardization of an orthotopic mouse brain tumor model following
830 transplantation of CT-2A astrocytoma cells. *Histol Histopathol.* 2007;22(12):1309-26.
831 65. Notta F, Doulatov S, and Dick JE. Engraftment of human hematopoietic stem cells is more efficient in female
832 NOD/SCID/IL-2Rgc-null recipients. *Blood.* 2010;115(18):3704-7.
833 66. Schaller TH, Snyder DJ, Spasojevic I, Gedeon PC, Sanchez-Perez L, and Sampson JH. First in human dose
834 calculation of a single-chain bispecific antibody targeting glioma using the MABEL approach. *J Immunother*
835 *Cancer.* 2020;8(1).
836 67. Torre D, Lachmann A, and Ma'ayan A. BioJupies: Automated Generation of Interactive Notebooks for RNA-Seq
837 Data Analysis in the Cloud. *Cell Systems.* 2018;7(5):556-61.e3.
838 68. Fernandez NF, Gundersen GW, Rahman A, Grimes ML, Rikova K, Hornbeck P, et al. Clustergrammer, a web-
839 based heatmap visualization and analysis tool for high-dimensional biological data. *Scientific Data.*
840 2017;4(1):170151.

841 69. Love MI, Huber W, and Anders S. Moderated estimation of fold change and dispersion for RNA-seq data with
842 DESeq2. *Genome Biology.* 2014;15(12):550.
843 70. Goedhart J, and Luijsterburg MS. VolcaNoseR is a web app for creating, exploring, labeling and sharing volcano
844 plots. *Scientific Reports.* 2020;10(1):20560.

845
846
847
848
849
850
851
852
853
854
855
856
857
858
859
860
861
862
863

Tables

Table 1. Demographics of hPBMC samples taken from healthy volunteers and glioblastoma patients

Characteristics	Control	Glioblastoma
	N = 5	N = 6
Age (yr)		
Median	54.3 (43.3–55.4)	58.7 (37.4–63.3)
Sex		
Male	2/5 (40%)	4/6 (66%)
Female	1/5 (20%	2/6 (33%)
Unknown	2/5 (40%)	0
Ethnicity		
American Indian/Alaska Native	0	0
Black or African American	0	0
Hispanic or Latino	0	0
Native Hawaiian or other Pacific Islander	0	0
Caucasian	3/5 (60%)	6/6 (100%)
Unknown	2/5 (40%)	0
Diagnosis		
IDHwt* glioblastoma	NA	6/6 (100%)
Newly diagnosed	NA	4/6 (66.7%)
Recurrent	NA	2/6 (33.3%)
Steroid Status		
Naïve	NA	1/6 (16.7%)
Experienced	NA	5/6 (83.3%)

*IDHwt: Isocitrate Dehydrogenase wild-type

Figures

Figure 1. IL-7-ALT CD8⁺ cells demonstrate increased accumulation within orthotopic glioblastoma models despite endogenous T cell sequestration in bone marrow

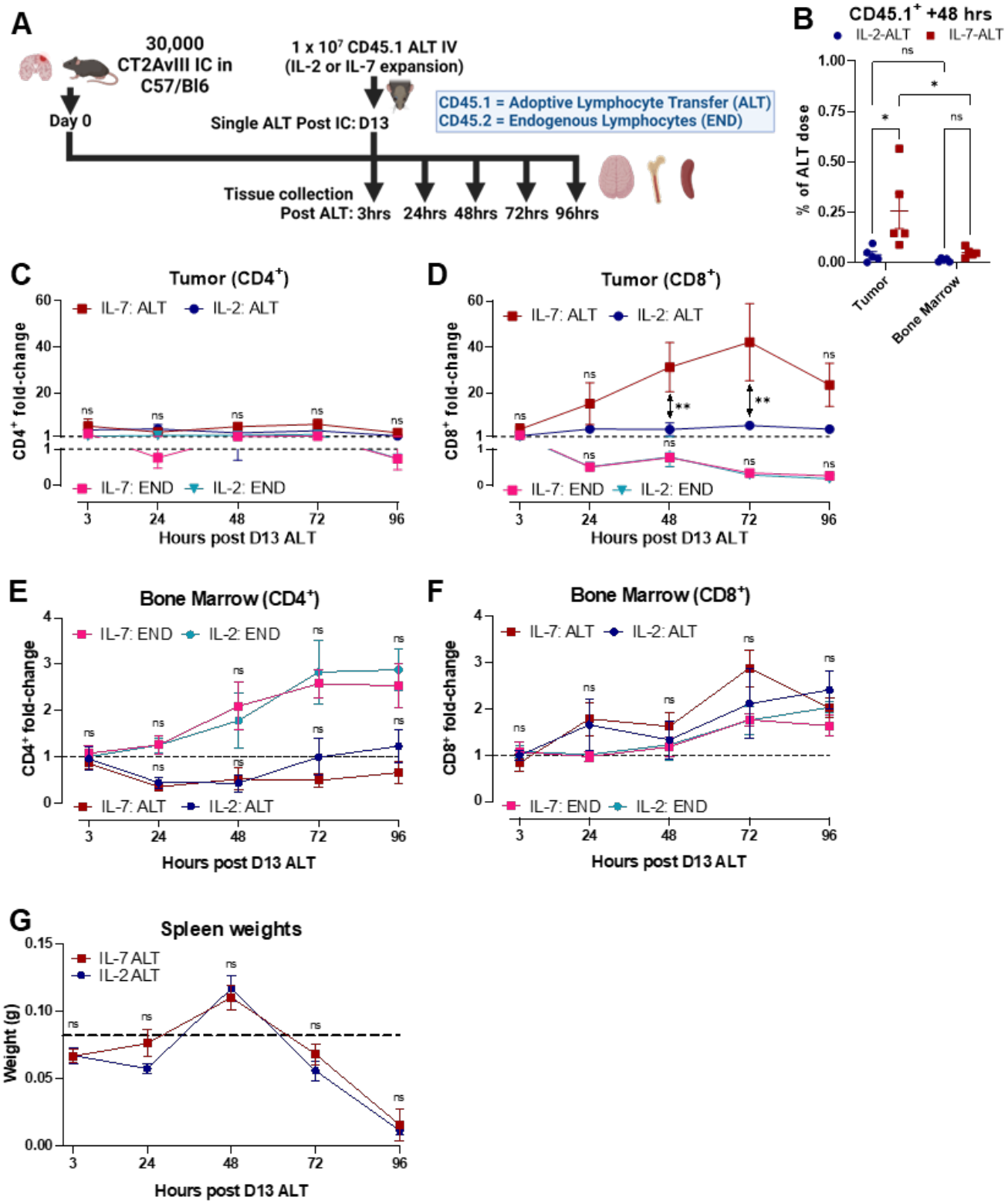

871 **(A)** Study overview (n=4-5 mice/group/time point for all graphs).

872

873 **(B)** Percentage of IL-2-ALT and IL-7-ALT CD45.1^{+} dose detected in tumor by 48-hours post administration (CD4^{+} & CD8^{+}

874 T cells).

875

876 **(C)** Fold-change relative to Day 0 of exogenous CD45.1^{+}CD4^{+} T cell entry and **(D)** CD45.1^{+}CD8^{+} T cell entry into brain

877 tumors.

878

879 **(E)** Fold-change relative to Day 0 of exogenous CD45.1^{+}CD4^{+} T cell entry and **(F)** CD45.1^{+}CD8^{+} T cell entry into bone

880 marrow.

881

882 **(G)** Time course of spleen sizes following ALT. Weights from control mice represented by dashed line (0.0823g, n=5).

883

884 Dashed line in C-F represents baseline (i.e., 1x). Statistical analyses performed via two-way ANOVA and data presented

885 as mean ± SEM unless otherwise specified. Experimental outline generated using BioRender.com.

886

887

888 Figure 2. IL-7-ALT synergizes with specific and non-specific T cell-activating/checkpoint blockade

889 therapies in orthotopic glioma models

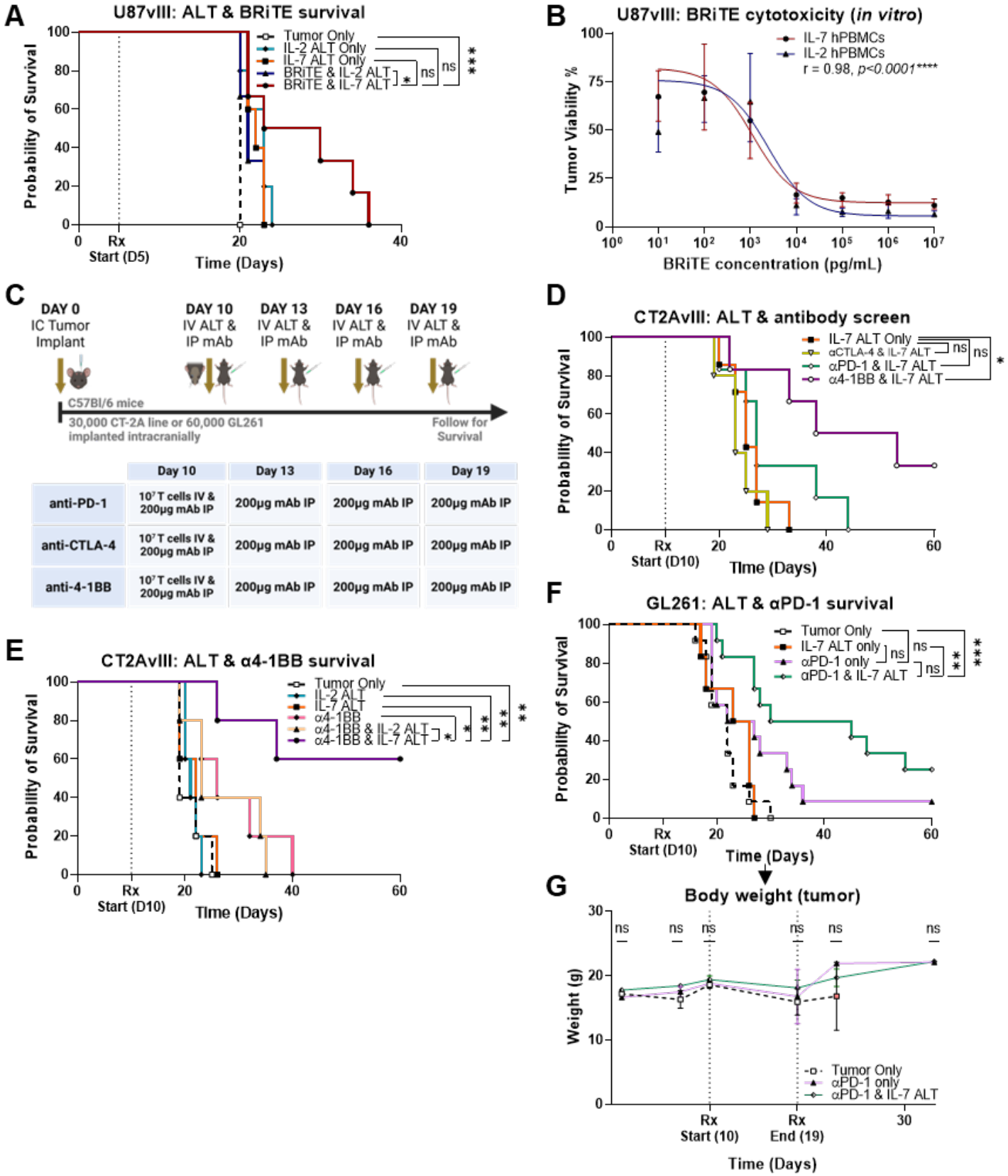

890

891 **(A)** Evaluation of IL-7 and IL-2 ALT combined with hCD3:EGFRvIII BRiTE in NSG mice. Mice (n=5-6 /group) were
892 implanted with U87vIII and treated with 5 x 10^6 IV hPBMCs on day 5, with serial IV BRiTE (50µg) on days 5-9.
893
894 **(B)** Cytotoxicity assay using BRiTE co-cultured with tumor cells (U87vIII) and hPBMCs expanded with IL-2 or IL-7. Non-
895 linear fitted dose-response curves shown with SEM (n=10-12/group, Pearson Correlation Coefficient r = 0.98,
896 p<0.0001****).
897
898 **(C & D)** Study overview and findings of a screening approach to identify the best combinatorial mAb approach with ALT
899 (n=5-7/group).
900
901 **(E)** Survival of combination α4-1BB & IL-7 ALT therapy compared to monotherapy controls treated using same regimen in
902 **(C)** (n=5/group).
903
904 **(F)** C57BL/6 mice implanted with 6 x 10^4 GL261 and treated using same regimen in **(C)** with αPD-1 (n=6-12/group, pooled
905 data across two experiments).
906
907 **(G)** Monitoring of bodyweight throughout the treatment period and for two weeks after for survival experiment in **(F)** (n=6-
908 7/group). Comparison via multiple unpaired t-tests and data presented as mean ± SEM.
909
910 Survival comparisons performed via Chi-Squared test. Experimental outlines generated using BioRender.com.

Figure 3. IL-7-expanded CD8⁺ T cells accumulating in tumor consist of both central and effector memory phenotypes

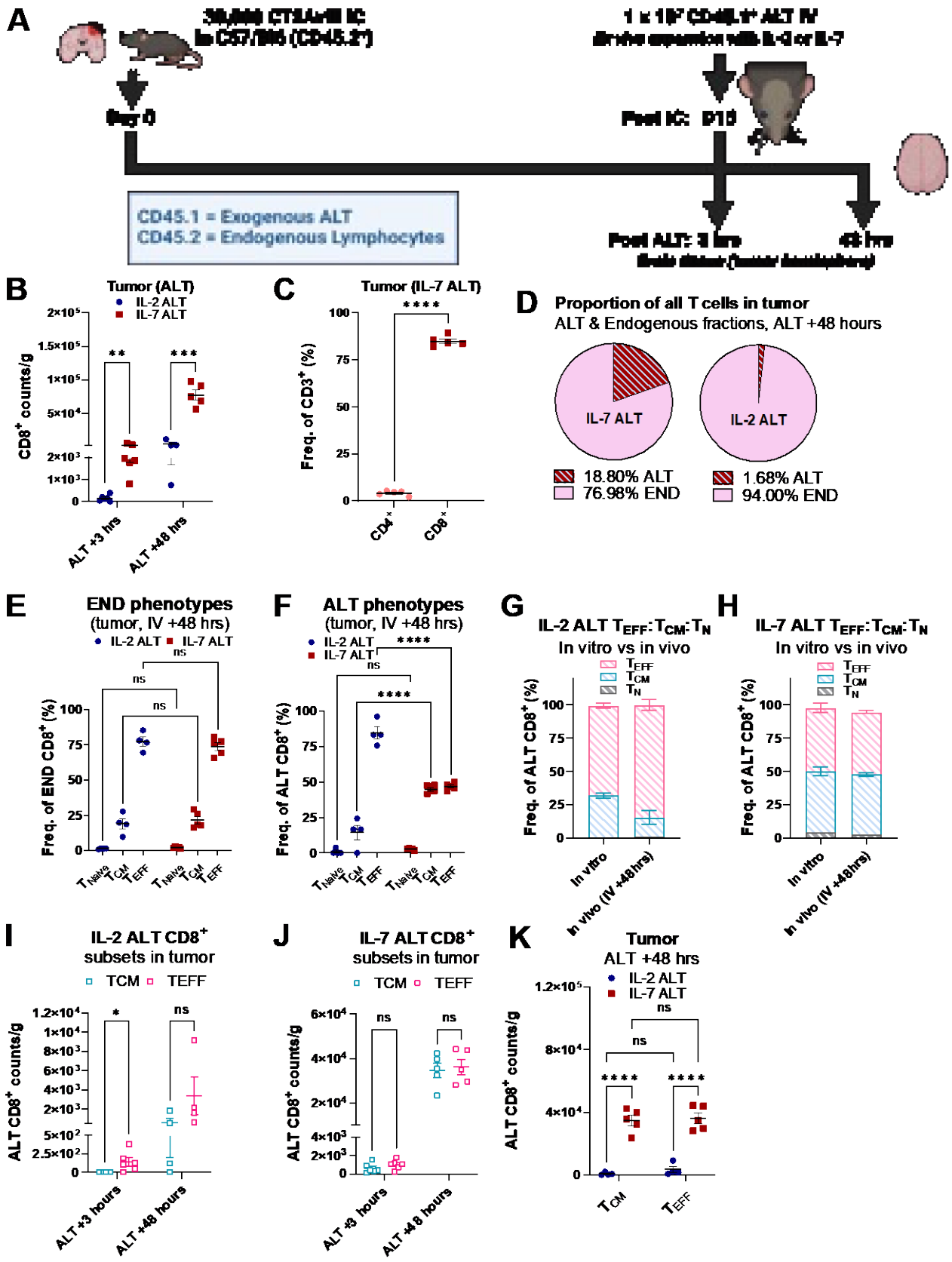

914 **(A)** Study overview in C57BL/6 mice (n=4-6/group for all graphs).

915

916 **(B)** Weight-adjusted counts of $CD45.1^+CD8^+$ T cells 3- and 48-hours following ALT in tumor (multiple unpaired t-tests
917 shown).

918

919 **(C)** Proportion of IL-7-ALT cells in tumor that are $CD4^+$ or $CD8^+$ T cells (unpaired t-test).

920

921 **(D)** Proportions of exogenous ALT to endogenous T cells in tumor 48-hours following administration.

922

923 **(E)** Comparison of Endogenous ($CD45.2^+$) or exogenous/ALT ($CD45.1^+$) **(F)** $CD8^+$ T_N, T_{CM}, T_{EFF} proportions between IL-2
924 and IL-7 ALT in tumor 48-hours following administration.

925

926 **(G & H)** Comparison of IL-2 and IL-7 ALT phenotype fractions in tumor to ALT pre-administration.

927

928 **(I & J)** Weight normalized counts at both 3- and 48-hr timepoints of $CD8^+$ T_{CM} and $CD8^+$ T_{EFF} accumulation in tumor when
929 treating with IL-2 or IL-7 ALT (multiple unpaired t-tests shown).

930

931 **(K)** Comparison of $CD8^+$ T_{CM} and $CD8^+$ T_{EFF} presence in tumor following IL-2-ALT or IL-7-ALT.

932

933 Statistical analyses performed via two-way ANOVA and data presented as mean ± SEM unless otherwise specified.
934 Experimental outline generated using BioRender.com.

935

936

937

938 Figure 4. Expansion with IL-7 upregulates expression of the pro-migratory integrin VLA-4 on murine

939 CD8⁺ T cells, which is required for enhanced intra-tumoral accumulation

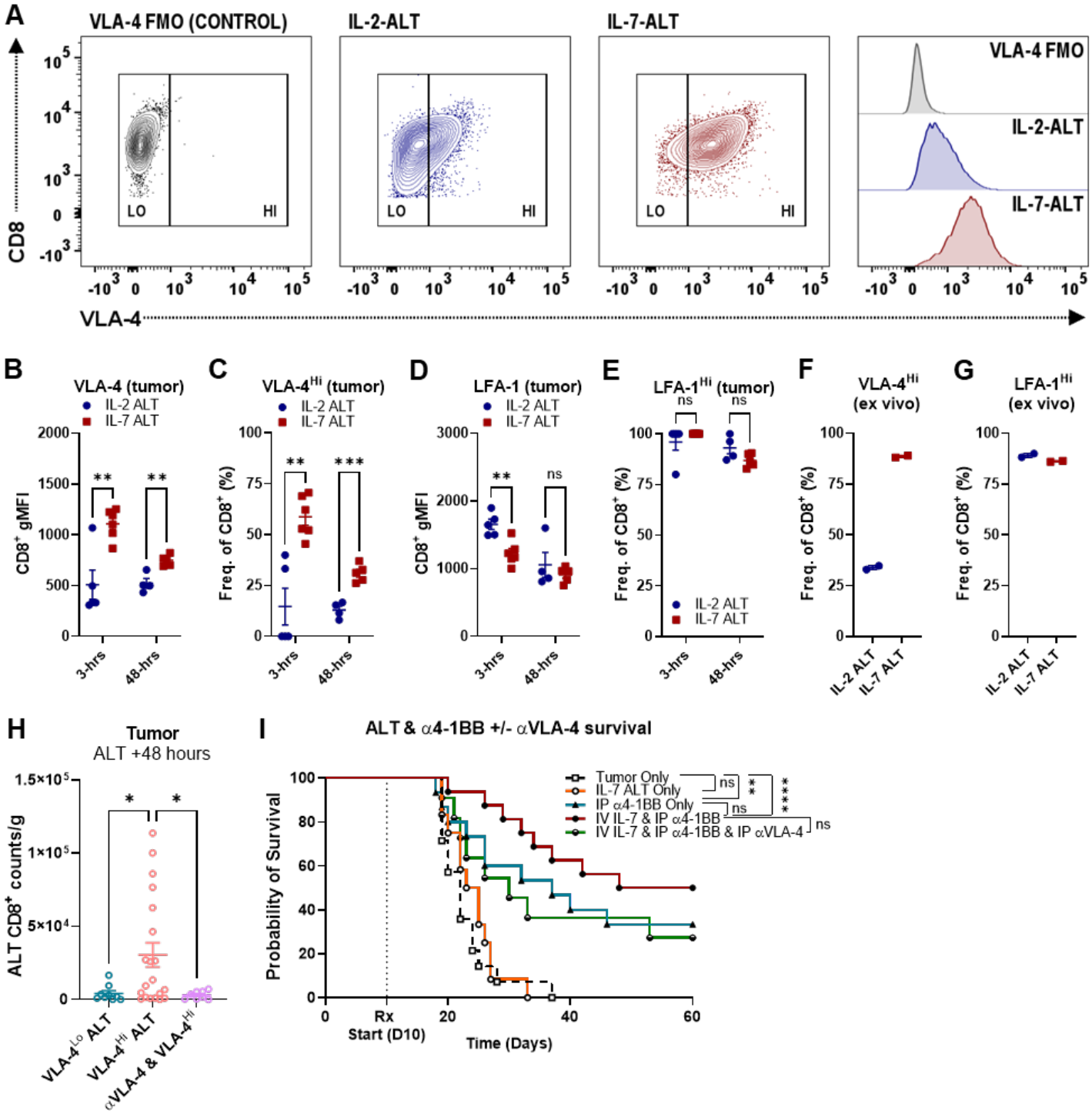

940

941

942

943

944 **(A)** Representative gating strategy shown for VLA-4 expression on $CD8^+$ T cells from IL-2 or IL-7 ALT.

945

946 **(B & C)** $CD8^+$ T cell VLA-4 expression (gMFI) and proportion of $CD8^+$ VLA-4^{Hi} T cells shown when expanding with IL-2 or
947 IL-7 ALT (experiment outline in Figure 3, n=4-6/group).

948

949 **(D & E)** $CD8^+$ T cell LFA-1 expression (gMFI) and proportion of $CD8^+$ LFA-1^{Hi} T cells shown when expanding with IL-2 or
950 IL-7 ALT.

951

952 **(F & G)** Analysis of the $CD8^+$ T cell VLA-4^{Hi} or LFA-1^{Hi} proportion in ALT cellular product at expansion end (2 technical
953 replicates).

954

955 **(H)** Entry of $CD45.1^+CD8^+$ T cells in tumor following VLA-4^{Lo}, VLA-4^{Hi} ALT or VLA-4^{Hi} ALT & αVLA-4 (single-dose 200μg
956 intraperitoneal αVLA-4 antibody (BioXCell) pre-ALT, 3 pooled experiments shown, n=8-20/group, one-way ANOVA shown).

957

958 **(I)** Evaluation of VLA-4 expression on the endogenous $CD8^+$ T cell compartment over time (IL-2 and IL-7 treatment groups
959 pooled, n=9-12/group). Survival comparisons performed via Chi-Squared test.

960

961 Statistical analyses performed using unpaired T tests and data presented as mean ± SEM unless otherwise specified.

962

963

964

965

966

967

968

969

Figure 5. Lymphocytic VLA-4 & endothelial/pericytic VCAM-1 expression increases over time on native T cells in murine glioma

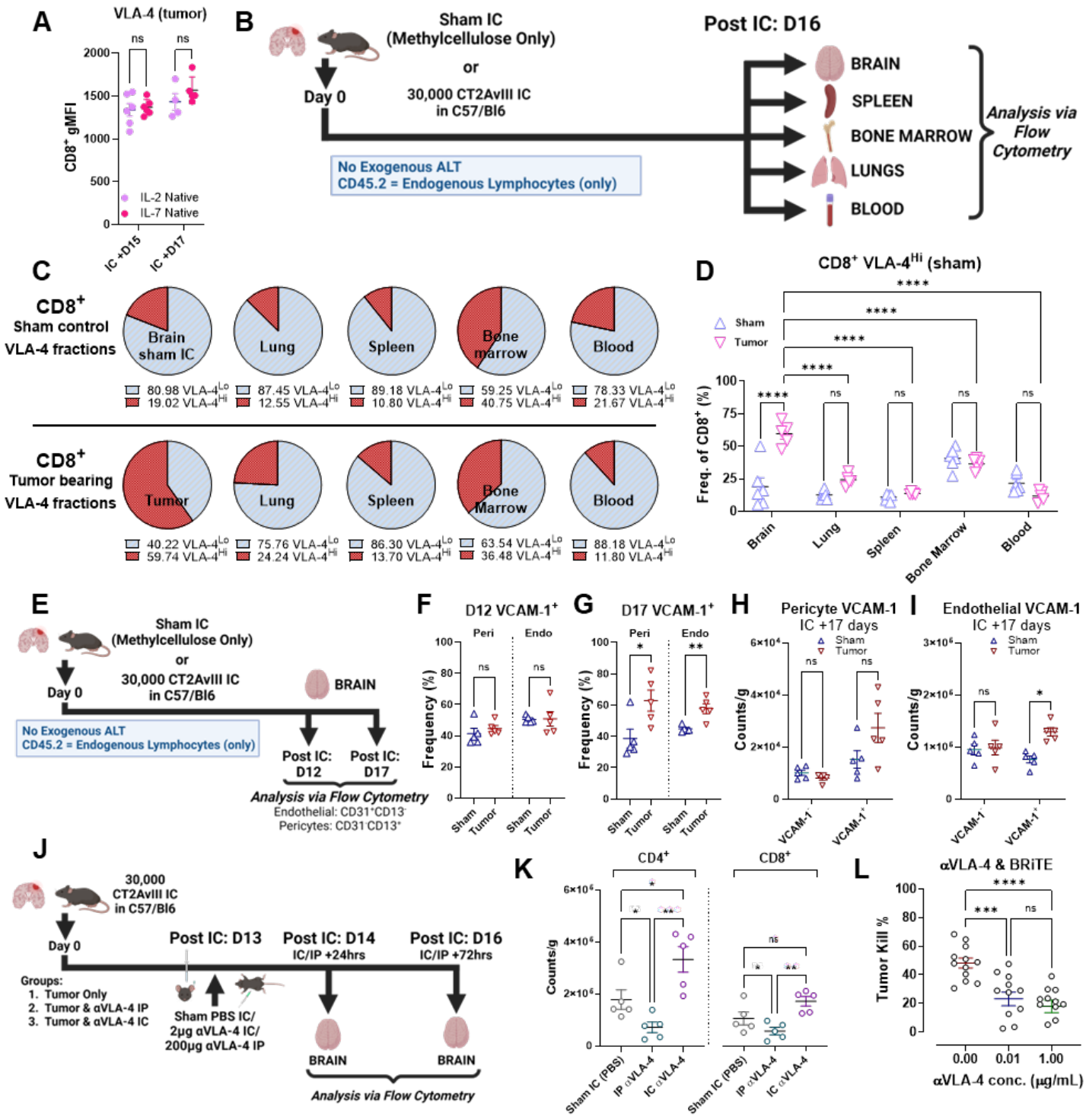

976 **(A)** Comparison of $CD8^+$ T cell VLA-4 gMFI expression on endogenous cells over time from prior experiment (n=4-6/group).

977

978 **(B)** Study overview to assess VLA-4 expression across compartments.

979

980 **(C & D)** Evaluation of VLA-4^{Lo} and VLA-4^{Hi} fractions across different compartments. Comparisons in **D** via two-way ANOVA

981 (n=5-6/group).

982

983 **(E)** Study overview to assess endothelial VCAM-1 in the CNS. No ALT was used. Tumor hemispheres were collected, and

984 endothelial cells ($CD31^+CD13^-$)/pericytes ($CD31^-CD13^+$) were analyzed (n=5/group).

985

986 **(F & G)** Frequency of VCAM-1^+ pericytes/endothelial cells in tumor at D12 and D17 following tumor/sham injection.

987

988 **(H & I)** Counts of VCAM-1^-/VCAM-1^+ pericytes/endothelial cells in tumor compared to sham controls at D17 following

989 intracranial injections.

990

991 **(J)** Study overview to evaluate intraperitoneal/intracranial VLA-4 blockade (n=5/group).

992

993 **(K)** Intracranial $CD4^+$ & $CD8^+$ T cell counts 72-hours following administration of intraperitoneal/intracranial αVLA-4 or sham

994 controls. Comparisons via one-way ANOVA.

995

996 **(L)** In vitro cytotoxicity with CT2AvIII, T cells, αVLA-4 and BRiTE at EC_{50} concentration of 0.01μg/mL. n=12/dose level.

997 Comparisons via one-way ANOVA.

998

999 Statistical analyses performed using unpaired T tests and data presented as mean ± SEM unless otherwise specified.

1000 Experimental outlines generated using BioRender.com.

1001

Figure 6. IL-7 expansion of hPBMCs from both healthy volunteers and patients with glioblastoma upregulates lymphocytic VLA-4 expression

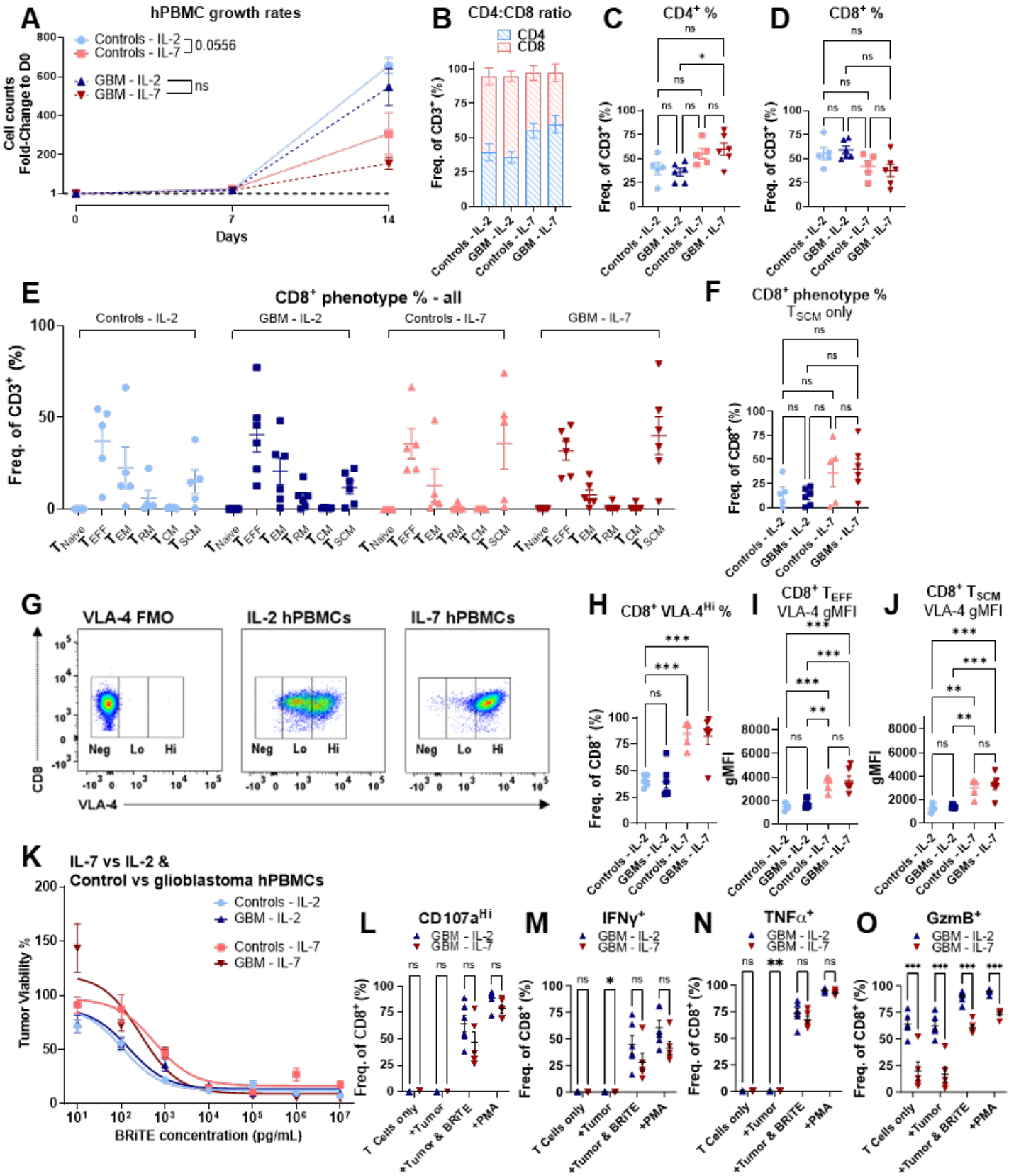

1005 **(A)** hPBMC growth rates for IL-2 vs IL-7 co-culture from both glioblastoma and control volunteer leukaphereses. (n=5-
1006 6/group).
1007
1008 **(B-D)** $CD4^+$:$CD8^+$ T cell ratios and comparisons for IL-2 vs IL-7 for control and glioblastoma samples at expansion end. **C**
1009 & **D**. Comparisons via one-way ANOVA.
1010
1011 **(E)** Overview of $CD8^+$ T cell phenotype fractions at expansion end: Naïve (T_N), Effector (T_{EFF}), Effector Memory (T_{EM}),
1012 Resident Memory (T_{RM}), Central Memory (T_{CM}), Stem Cell Memory (T_{SCM}).
1013
1014 **(F)** Fraction of $CD8^+$ T_{SCM} at expansion end across groups.
1015
1016 **(G-J)** Gating strategy for VLA-4^{Hi} fraction and proportion of VLA-4^{Hi} in all $CD8^+$ T cells (**H**) as well as $CD8^+$ T_{EFF} (**I**) and
1017 $CD8^+$ T_{SCM} cells (**J**) at expansion end.
1018
1019 **(K)** Cytotoxicity assay with tumor (U87vIII) co-cultured with IL-2 or IL-7 expanded donor/glioblastoma hPBMCs & BRiTE.
1020
1021 **(L-O)** Degranulation assays assessing $CD107^{Hi}$, $GzmB^+$, $IFN\gamma^+$, $TNF\alpha^+$ in glioblastoma $CD8^+$ T cells expanded with IL-2
1022 and IL-7. Comparisons via multiple unpaired t tests (n=5-6/group).
1023
1024 Statistical analyses performed using one-way ANOVA and data presented as mean ± SEM unless specified.
1025
1026
1027
1028
1029
1030
1031
1032

Figure 7. IL-7 upregulates transcription of genes associated with enhanced migratory integrin expression (*CD9*) and protection against tumor-induced sequestration (*S1PR1*)

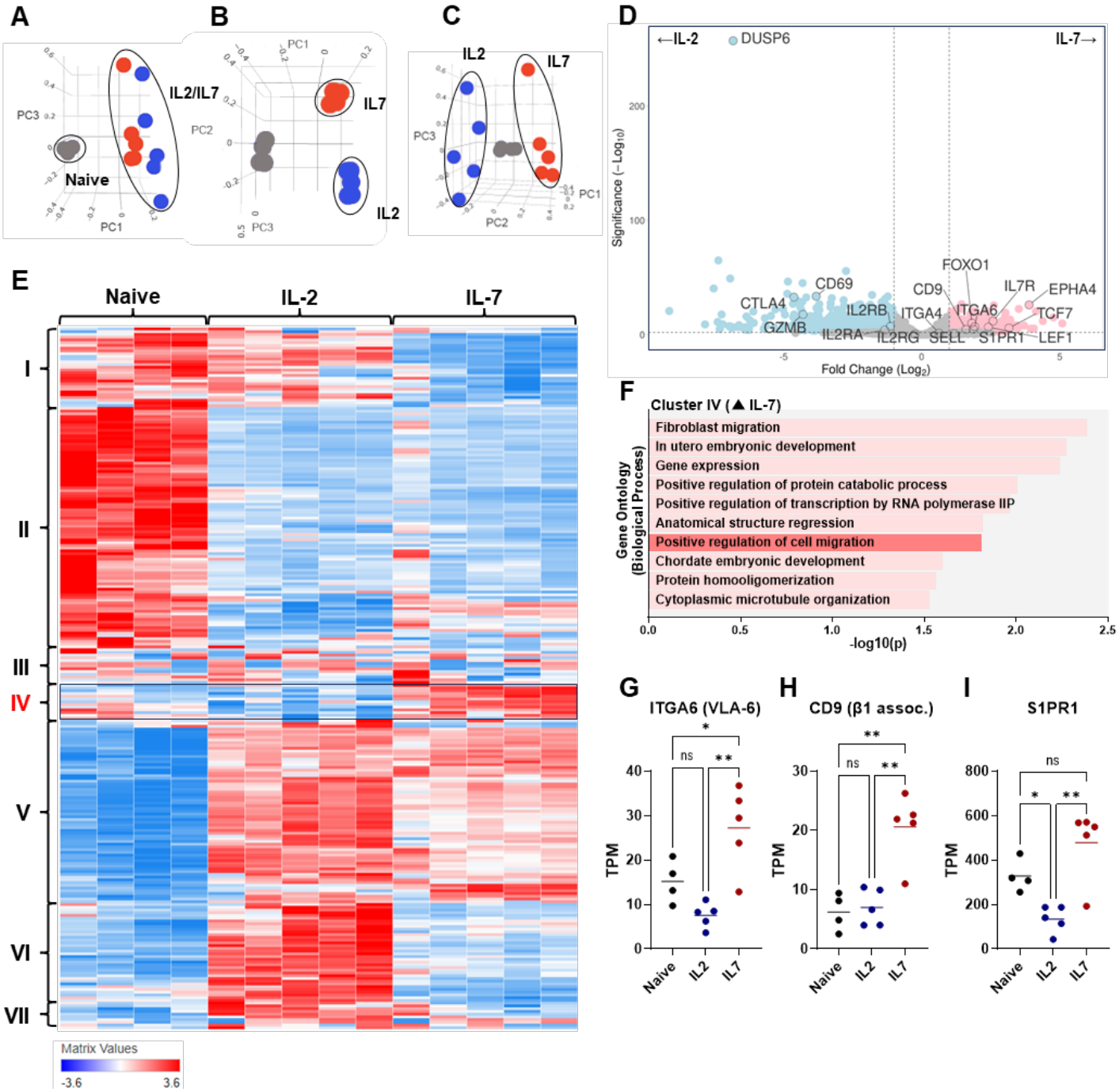

1039 **(A-C)** Principal component analysis of naïve (grey), IL-2 expanded (blue) and IL-7 expanded (red) $CD8^+$ T cells (n=4-
1040 5/group for all graphs).
1041
1042 **(D)** Volcano plot comparing differential gene expression between IL-2 and IL-7 expanded $CD8^+$ T cells.
1043
1044 **(E)** Hierarchical cluster heatmaps of the naïve, IL-2 and IL-7 groups with seven unique clusters identified (I-VII).
1045
1046 **(F)** Gene Ontology biological processes analysis of genes expressed in cluster IV (upregulated with IL-7, *EPHA4, CD9,*
1047 *ITGA6, S1PR1* etc.)
1048
1049 **(G-I)** Comparisons of raw transcripts per million (TPM) across groups for *ITGA6, CD9* and *S1PR1* (comparisons via one-
1050 way ANOVA).
1051
1052 PCA analysis was generated using BioJupies (67). Hierarchical cluster heatmaps were generated using clustergrammer
1053 (Maayan lab, (68)). Gene Ontology (GO) biological processes analysis was performed using the NIH DAVID database
1054 (54). Volcano plots were generated using VolcaNoseR (70). Comparisons via one-way ANOVA and data presented as
1055 mean ± SEM unless otherwise specified.
1056
1057
1058
1059
1060
1061
1062
1063
1064